GROUND-LEVEL INSOLATION

IN THE

UV-B SPECTRAL REGION

A THESIS PRESENTED IN PARTIAL FULFILMENT OF THE
REQUIREMENTS FOR THE DEGREE OF
MASTER OF SCIENCE
IN PHYSICS AT
MASSEY UNIVERSITY

by

BRUCE W. HARTLEY

1982

ABSTRACT

This thesis describes the design and construction of two instruments for use in isolating the ultraviolet parts of the Solar spectral irradiance at Earth's surface.

The first was a total UVA Pyranometer, which was undertaken to make preliminary investigations in the techniques of monitoring ultraviolet irradiances, as well as to provide useful data.

The main part of this thesis was the construction of a portable, easily operated, interference filter spectrophotometer to isolate the ultraviolet-B spectrum into five discrete 10 nm passbands. However, as further reading will describe, realisation of only the two longer wavelength passbands was made due to deviations from the ideal quasi-rectangular passbands of the interference filter spectral transmittance curves. Discussion of how these problems can be overcome is presented in the conclusion. An outline on how the incident spectral solar irradiance could be found, from the five passbands, is presented along with some preliminary data from the two operational channels. An overall accuracy of 15% was obtained for data obtained, with better accuracies, to 7%, attainable by stabilisation of the instrument power supplies and, therefore, output voltage.

ACKNOWLEDGEMENTS

Many thanks go to my supervisor Dr. R.K. Lambert for providing the topic about which this thesis is based, and providing many hours of interest and support during its construction. Also Mr E.R. Hodgson and the Massey University physics staff for assisting with ideas in the preliminary stages of the instrument constructions. The University workshop technicians provided invaluable assistance in supplying materials and equipment required in the design and construction, and the assistance of staff at the Physics and Engineering Laboratories, Gracefield, the New Zealand Meteoroligical Service, Wellington, and the Plant Physiology Division of the D.S.I.R., Palmerston North, in field testing and calibration of the instruments. Thanks also to my wife, Sharon, for her patience and support during the writing of this thesis, and to the typists Mrs Diane Burns, Mrs Rosalie Heap and Miss Kirsty Rutherford.

TABLE OF CONTENTS

LIST OF FIGURES

LIST OF TABLES

GLOSSARY

a,b,c,	: Constants.
a_λ	: Optical thickness of atmosphere in the zenith direction.
A	: Attenuator and attenuation coefficient.
$A_{aperture}$	: Area of aperture.
A_D	: Area of diffuser that is irradiated.
A_k	: Area of photocathode that is irradiated.
c	: 3×10^8 m s^{-1}.
C	: Calib-ration constant of UVA instrument.
dh	: Length of a column of atmosphere in the zenith direction.
ds	: Lenght of a column of atmosphere in the solar direction.
D_1	: Diode one.
D_n	: Dynode number n.
D_λ	: Spectral transmittance of the protective dome.
e	: Elementary charge.
e_o	: Output voltage of UVA instrument.
E	: Integrated irradiance over bandwidth $\lambda_2 - \lambda_1$.
EHT	: High voltage.
E_D	: Irradiance at the diffuser.
$E_{instrument}$	: UVB instrument output for irradiance by the monochromator.
$E_{o,instrument}$	: Normalising value of $E_{instrument}$.
E_k	: Irradiance at the photocathode.
E_n	: Total irradiance received by channel n.
$E_{n,o}$	: Normalising value of E_n.
E_{output}	: Calibrating PMT output for irradiance by the monochromator.
$E_{o,output}$	: Normalising value of E_{output}.

E_{pmt} : Irradiance from the calibration monochromator.

$E_{o,pmt}$: Normalising value of E_{pmt}.

E_{solar} : Total integrated solar irradiance.

$E_{s,n}$: Solar spectral irradiance of channel n.

E_{uvA} : Integrated irradiance over the UVA band.

$E_{k,max}$: Maximum total irradiance allowable at the photocathode.

$E_{o,n}$: Total integrated irradiance of channel n after weighting of the incident spectral irradiance by the normalised spectral sensitivity of that channel.

$E_{o,\lambda,max}$: Maximum spectral irradiance allowable at the diffuser.

E_{λ} : Solar spectral irradiance of Earth's surface.

$E_{\lambda,n}$: Spectral irradiance of channel n.

$E_{\lambda,k,max}$: Maximum spectral irradiance allowable to the photocathode.

$E_{\lambda,o,n}$: Approximation of the spectral irradiance of channel n.

F : Filter.

F_{λ} : Filter spectral transmittance.

FF_n : Filter factor of channel n.

F : Effective bandwidth of UVB instrument filters.

F_n : Bandwidth of channel n filter.

G : Gain of PMT in A/lm.

h : Planck's constant.

i : Total photocathode current.

i_d : Dark current.

i_k : Photoemissive current.

$i_{k,max}$: Maximum photocathode current allowable.

i_o : Normalising value of i.

$i_{\lambda,k}$: PMT photocathode current for irradiance at wavelength λ .

I	: Integrated anode current over bandwidth $(\lambda_2 - \lambda_1)$.
ICX	: Integrated circut number X.
I_{Dark}	: PMT anode dark current.
$I_{o,\lambda}$	: Incident monochromatic radiation intensity.
I_{λ}	: Transmitted monochramtic radiation intensity.
$I_{\lambda,A}$	: PMT anode current for irradiance at wavelength λ.
K,K^1	: Calibration constants for the UVB instrument.
M	: PMT overall sensitivity in A/lm.
M_r	: Relative air mass.
P	: Denormalisation factor.
PMT	: Photomultiplier tube.
PT	: Photoemissive tube.
q	: Quartz diffusing disc.
Q_1	: Transistor number one.
Q_{λ}	: Photocathode quantum efficiency.
r	: Dimension of atmosphere particle.
r	: Source - detector distance.
r_o	: Normalising value of the source - dector distance.
R	: Resistance in ohms.
RC	: Resistor - Capacitor.
RX	: Resistor number X.
s_{λ}	: Spectral sensitivity of the photocathode.
S	: Integrated sensitivity over bandwidth $(\lambda_2 - \lambda_1)$.
S_o	: Normalising value of S above.
S	: Solar position.
$S_{\odot}$	: Solar angle.
S_x	: Switch number X.
S_{λ}	: Total spectral sensitivity.
$S_{\lambda,n}$	: Spectral sensivity for channel n of the UVB instrument.
$S_{o,\lambda,n}$	: Normalised values of $S_{\lambda,n}$.
T	: Total effective transmittance of UVB instrument diffuser, protective dome and collimator.
T_D	: Effective diffuser transmittance.

T_{Delay} : Period of monostable delay pulse.

T_{sample} : Period of monostable sample pulse.

UV : Ultraviolet.

UVA : Ultraviolet A radiation.

UVB : Ultraviolet B radiation.

UVC : Ultraviolet C radiation.

V : UVB instrument output voltage.

V_o : Normalising value of V.

V_{EHT} : High voltage applied to the PMT.

Z : Zenith position.

$Z_\odot$: Zenith angle.

θ : Angle from the normal of the diffuser surface.

: Wavelength.

λ_o : Wavelength of the irradiance $E_{o,pmt}$.

λ_1 : Lower limit of bandwidth.

λ_2 : Upper limit of bandwidth.

Π : Unit of angular measurement, $\Pi = 3.141$.

ϕ_k : Spectral radiant power at the PMT photocathode.

ϕ_{UVA} : Integrated radiant power within the UVA band.

ϕ_λ : Spectral radiant power at the photocathode.

Ω : Solid angle subtended by the dector from the centre of the diffusing disc.

CHAPTER 1

Introduction

The importance of UV (ultraviolet) radiation that reaches Earth's surface is clearly seen when the action spectrum and effectiveness in the destruction of organic materials and biological tissues is observed. Fig:1.1 [1]* clearly illustrates this importance. Other effects of UV radiation include destruction of the genetic material (DNA), induction of skin cancers, eye inflamation and migration of melanin from lower to upper layers of skin as a form of protection known as tanning. Destruction of bacteria in skin diseases and sterilisation processes, and the production of vitamin D are some of the beneficial effects. Exposure of plants to intense UV is usually fatal, and lesser doses induce tumors, enhance genetic defects, stop photosynthesis and cause severe damage to outer leaf cells. Many insects use UV light as an "extended vision" for navigation, and food and predator recognition. This extended vision is exploited by humans in lures to capture insects for pest destruction or examination. Industrial organic materials such as rubbers and plastics break down after prolonged UV exposure and are rendered worthless.

In the erythemal region of the UV, which can cause severe sunburning, it is interesting to observe the fallacies of some common beliefs about protection from the UV. Light colourful summer shirts can transmit up to 75% of the incident radiation, a one meter column of sea water transmits approximately 60% of radiation at 310 nm, and shady areas can receive large UV irradiances from diffuse sky radiation.

The UV spectrum from the sun has been subdivided into three sections of which two main classifications are presented in the literature.

* Numerals in square brackets refer to entries in the bibliography

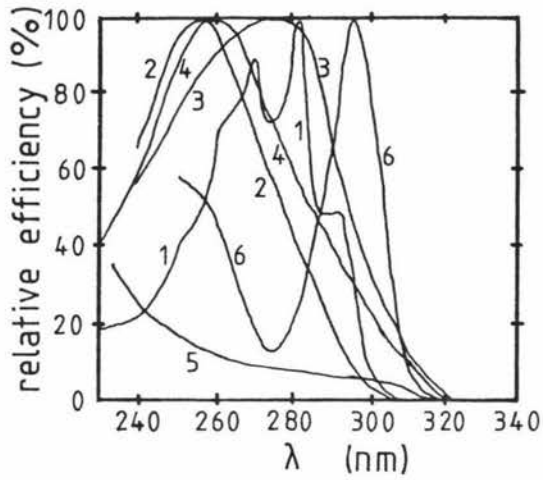

Fig :1-1 Biological effects of ultraviolet radiation[1].
(1)Production of vitamin D,(2)bactericidal effects,
(3)stoppage of tissue growth,(4)albumen coagulation,
(5)haemolysis,(6)erythema.

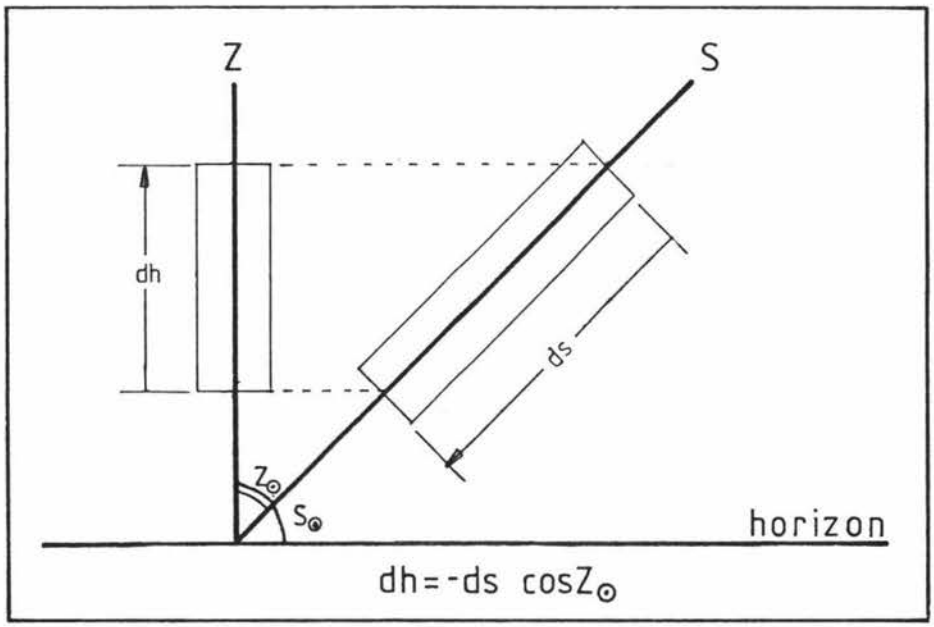

Fig :1-2 Bouger-Lambert law :diagramatic representation.

S :solar position $S_\odot$:solar angle

Z :zenith position $Z_\odot$:zenith angle

Table I

Ultra-Violet Wavelength classifications.

λ(nm), classification A [2,3]		λ(nm), classification B [4]	
1-200	far UV	1-280	UVC
200-300	middle UV	280-320	UVB
300-400	near UV	320-400	UVA

Classification B, which is now the more commonly used, will be used in this thesis. The reasons for subdivision of the UV into the UVA, UVB and UVC become apparent when considering the radiation which reaches Earth's surface.

UVA: The atmosphere is relatively transparent to wavelengths of this region, and the radiation is weakly biologically active.

UVB: Transmission of this radiation is very dependent on the amount of ozone in the upper atmosphere. These wavelengths of radiation are responsible for erythema and most other biological effects.

UVC: No solar radiation of wavelength less than approximately 280 nm penetrates the atmosphere because of ozone and oxygen absorption.

Before reaching Earth's surface the Sun's radiation undergoes many modifications. Variation of the Earth-Sun distance causes an approximate 6% variation of the incident irradiance. Scattering and absorption in Earth's atmosphere, and reflection and radiation from Earth's surface also cause changes in the irradiance and polarization received at Earth's surface.

Scattering and Absorption

Prediction of atmospheric transmission is achieved by considering two columns of equal cross section in the atmosphere, one in the zenith direction and one in the solar direction.

The Bouger-Lambert law, equation (1.1), [1] expresses the relation between incident and transmitted radiation intensities.

$$I_\lambda = I_{0,\lambda} \exp(-a_\lambda M_r) \qquad (1.1)$$

$$M_r = \frac{-ds}{dh} = \sec Z_\theta$$

$I_{0,\lambda}$ Incident monochromatic radiation intensity on to column ds.

I_λ: Transmitted monochromatic radiation intensity by column ds.

a_λ: Optical thickness in zenith direction (extinction or attenuation coefficient).

M_r Relative air mass of columns assuming constant atmospheric densities.

This theory neglects atmospheric curvature and refractive index changes between layers of the atmosphere at different temperatures and densities and, therefore, gives results which are valid only for high solar angles.

Scattering is responsible for the polarization of diffuse sky radiation, and the variation of scattering coefficients with wavelength gives a diffuse sky spectrum different from that of the direct radiation. This dependence of coefficient on wavelength is described by the Rayleigh and Mie relations and, for longer wavelengths, by geometrical optics. The criterion for Rayleigh scattering is that the characteristic dimension of the aerosol, r, obeys the condition $r \leq 0.1\lambda$, where λ is the wavelength of the radiation incident on the aerosol particle. When this is satisfied the coefficient is proportional to λ^{-4}. This illustrates why a clear diffuse Rayleigh sky is blue, and the thicker the optical path the more the blue light is scattered out of the direct beam. This is seen at sunset with a red sun and deep blue diffuse sky radiation. As the wavelength gets shorter (into the UV) the scattering coefficient increases, and experiments [5] indicate that as much as 60% of the radiation in the UVB is received from the diffuse sky. For larger particles, $0{\cdot}1\lambda \leq r \leq 25\lambda$, the Mie theory describes the scattering, and for $r \geq 25\lambda$, geometrical optics can be used. With increasing particle size the scattering coefficient becomes less wavelength-dependent; the effect is seen in a whitening of smog, dust and cloud laden skies.

Absorption of UV radiation by atmosphere gases is of great importance because of the destructive effects that would be produced by an increase in the UV at Earth's surface. Most important of the atmospheric gases is ozone which lies in the upper atmosphere, with peak concentration occurring between 10 and 40 km altitude and decreasing up to 90 km [2]. Even though the amount of ozone is small in comparison to the total atmosphere, (several millimeters of ozone at standard temperature and pressure compared to 8 km of total atmosphere) it has very strong photo-chemical properties in which UV radiation is absorbed. The main absorption occurs in the Hartley bands which extend from 200 to 320 nm and affect the UVB reaching Earth's surface. The Huggins bands cover 320 to 360 nm and affect the UVA but with less absorption than the Hartley bands. It is the ozone absoprtion that is responsible for the sharp cut-off with decreasing wavelength of the radiation spectrum observed at Earth's surface.

The information presented here illustrates the need for data from routine monitoring instruments, to provide a base line from which predictions of the effects of changes in UV insolation can be made. It follows that reliable instruments are required to provide this data, and to date instrumentation has failed to meet the requirements of large scale, consistent, spectral measurements of the UV that reaches Earth's surface. In this thesis, two such instruments will be described which have the capability of providing this baseline data. In chapter 2 a UVA pyranometer is described. This instrument provides information on the total UVA irradiance incident on a flat surface. A filter wheel based instrument is described in chapter 3. The data from this instrument can provide information on the spectral dsitribution of the irradiance received on a flat surface in the UVB band.

CHAPTER 2

UVA Pyranometer

All radiometric instruments are constructed from a similar set of Functional blocks, namely, a collector to sample the required part of the sky's radiation, filters for spectral isolation, a detector to convert the irradiance into a readable signal, and electronics to run the detector and recording mechanism.

To gain more knowledge of the practical application of these basic functions,and to provide data for later comparison, a simple UVA pyranometer was constructed. The design arrived at is shown in Fig: 2.1. The transducer consists of a diffusing disc to simulate a flat plate detector response and two nickel salt impregnated glass filters to provide the appropriate UVA passband for detection by the photo-tube. The attenuator is included to keep the irradiance, at the photocathode, within the designed operating region of the photo-tube at the working voltage provided by the high voltage supply. The resultant photo-current is sensed by a current-to-voltage converting operational amplifier and the resultant signal is stored on suitable recording apparatus. Detailed description of each functional block now follow.

2.1 Description of the Instrument

Diffuser

By definition, an ideal diffuser re-radiates evenly over 4π steradians all incident irradiance. Of this diffused radiation the detector samples a constant portion, and the diffuser can, therefore, be considered to act as a neutral density filter with a cosine collecting response. The effective transmittance of the diffuser to detector is found from the expression

$$T_D = \frac{E_k}{E_D} = \frac{A_D}{A_k}\,\frac{\Omega}{4\pi} \qquad (2.1)$$

A_D : Area of diffuser that is irradiated
A_k : Area of photo-cathode irradiated
E_k : Irradiance at photo-cathode
E_D : Irradiance at diffuser

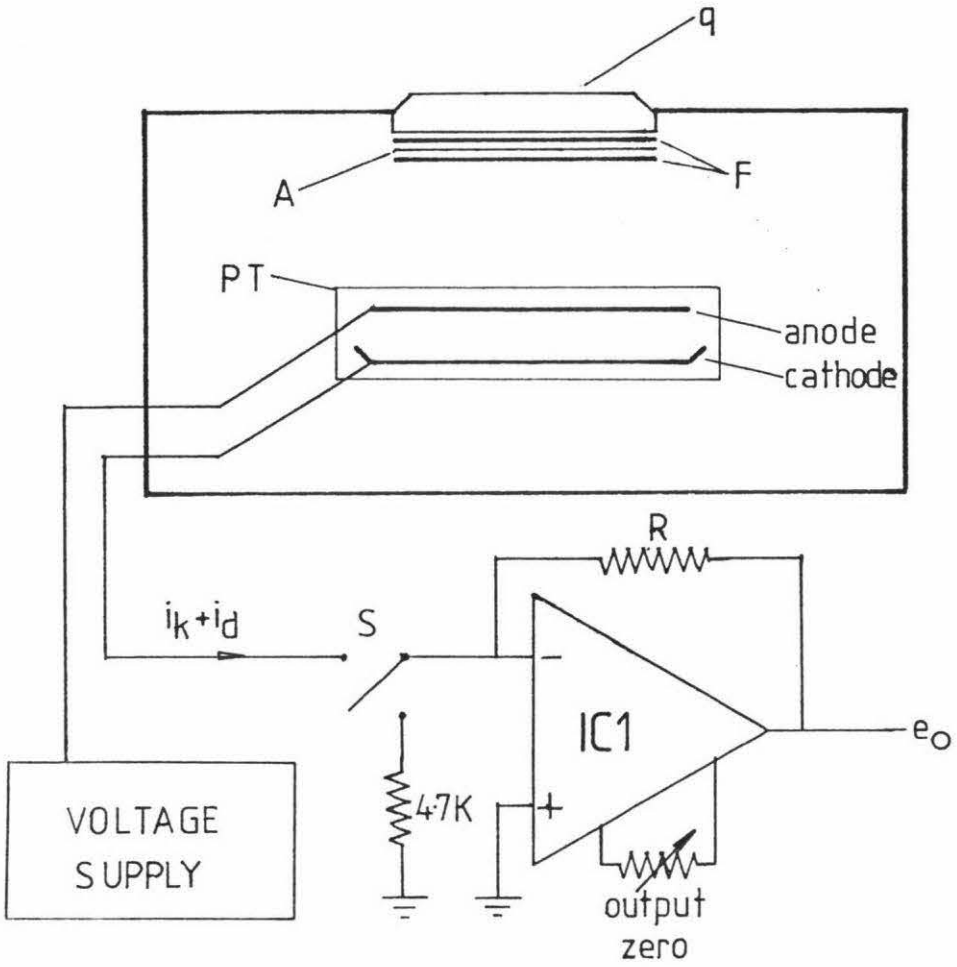

Fig:2·1 UVA PYRANOMETER

i_k : photocathode current.

i_d : dark current.

PT : photoemissive tube.

A : attenuator.

F : filter.

q : quartz disc.

Ω : Solid angle subtended by the detector from the centre of the diffusing disc.

In the derivation of equation (2.1) the following assumptions were used:

(I) Diffusing disc has no absorbance.
(II) Re-radiation of incident irradiance is from an isotropic point source at the center of the diffuser.
(III) Single scattering of light in disc.

Because of large deviations from these assumptions the resulting effective transmittance of the diffuser is used only as a guide-line in the initial design of the instrument. From equation (2.1) the value of T_D was found to be $T_D = 0.08$

where $A_D = (1.26 \pm 0.06) \times 10\ cm^2$

Filters

The filters used were Leybold 46979 and were 2 mm in thickness. To give the desired spectral passband and a better signal-to-noise ratio of passband radiation to that outside the passband, two of the filters were used and the resultant spectral transmittance (F_λ) is seen in Fig: 2.2. These filters also have a passband in the infra-red spectral region but the detector chosen has zero response at these wavelengths and it can, therefore, be ignored.

Attenuator

To lower the irradiance levels at the detector cathode to within design operating limits, an attenuator was placed between the diffuser and detector. Stainless steel gauze [6] was used because of its nearly constant transmittance over the wavelength range of the instrument. From equations (2.3) and (2.4) it was predicted that an attenuator of transmittance 3.5×10^{-4} would be required. By experiment, three gauzes were required however, and they have a total transmittance of $A=(5.8 \pm 0.4) \times 10^{-2}$ as measured, (as are all spectral measurements in this thesis, unless otherwise stated) on a Shimadzu MPS 500 spectrophotometer with beam size 12 mm by 3 mm. This area of illumination is very large in comparison to the gauze dimensions and, therefore, an effective average transmittance is found. The

gauze dimensions are: wire diameter (0.007 ± 0.002)cm, and wire spacings (0.014 ± 0.002) cm in both binding directions.

Detector

A photoemissive tube, type 92AV by Mullard, with an S-11 response was used [7] . It was assumed, for the purpose of instrument initial design calculations, that the quantum efficiency of the 92AV was the same as for the photocathode of the photomultiplier in chapter 3. Deviations from the approximation are expected due to the different device geometries and operating voltages. The spectral sensitivity of the detector is expressed as

$$s_\lambda = i_k / \phi_\lambda$$

$$= \lambda Q_\lambda e / hc$$

$$= 8.065 \times 10^5 \times \lambda Q_\lambda \ (A\ W^{-1}\ nm^{-1}) \qquad (2.2)$$

s_λ : Spectral sensitivity of the photocathode at wavelength λ.
λ : Wavelength of incident irradiance.
e : elementary charge
h : Planck's constant
c : 3×10^8 ms^{-1}
ϕ_λ : radiant power at the photocathode
Q_λ : Photocathode quantum efficiency [7,8] which is shown in Fig: 2.2.

The spectral sensitivity of the total transducer is now found from the expression

$$S_\lambda = T_D\, A F_\lambda\, s_\lambda \qquad (A\ W^{-1})$$

(T_D and A were defined in connection with equation (2.1)). The integrated sensitivity over the bandwidth $(\lambda_2 - \lambda_1)$ is given by equation (2.3)

$$S = \int_{\lambda_1}^{\lambda_2} S_\lambda \, d\lambda$$

$$= 8.065 \times 10^5\, T_D\, A \int_{\lambda_1}^{\lambda_2} \lambda F_\lambda\, Q_\lambda \, d\lambda \qquad (2.3)$$

The integral was evaluated numerically from Fig: 2.3

$$\int_{\lambda_1}^{\lambda_2} \lambda\, F_\lambda\, Q_\lambda \, d\lambda = (1.77 \pm 0.05) \times 10^{-6} \ (m)$$

and thus $S = (6.6 \pm 1.5) \times 10^{-3}\ (A\ W^{-1})$

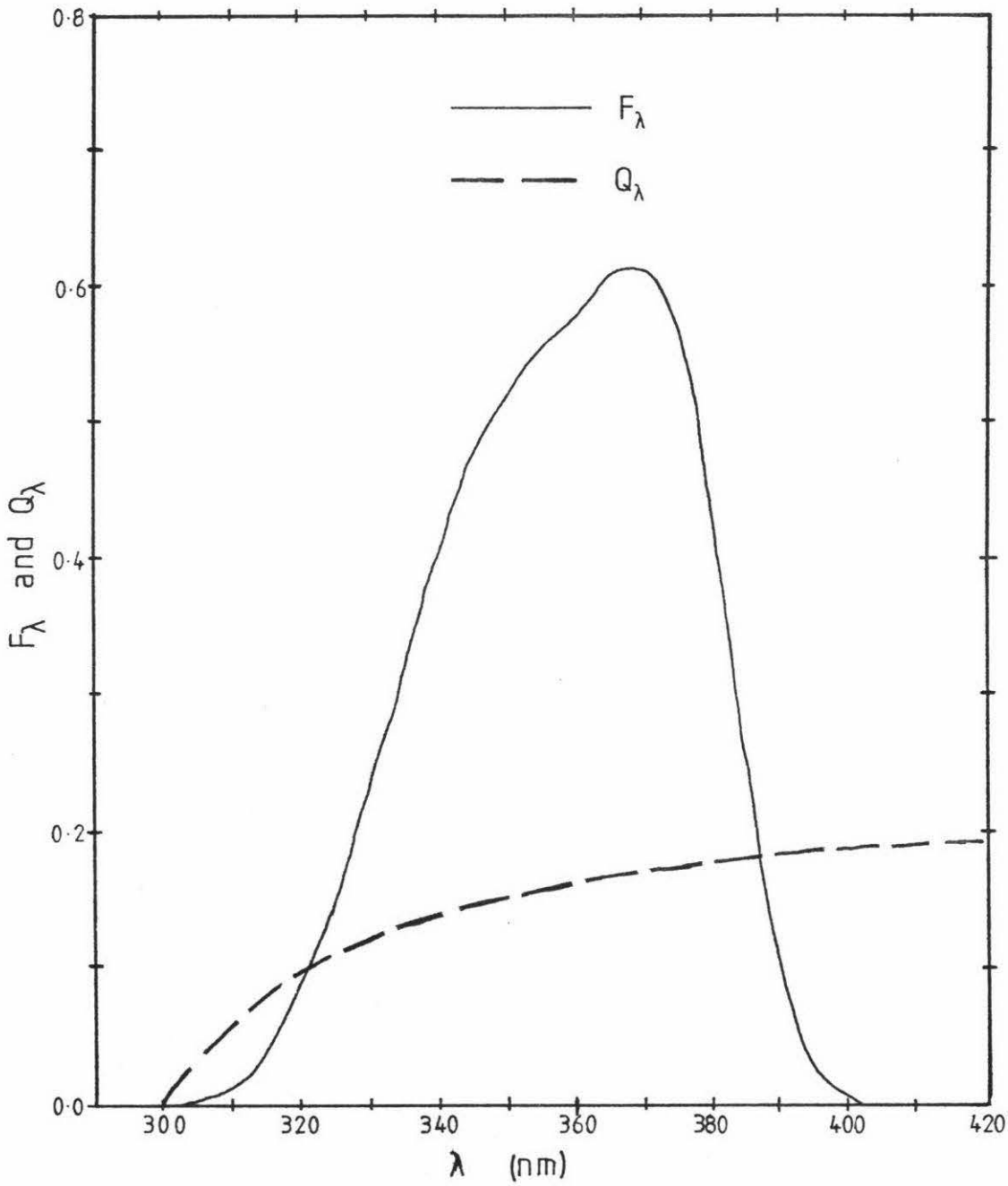

Fig:2-2 UVA filter transmittance and photocathode quantum efficiency.

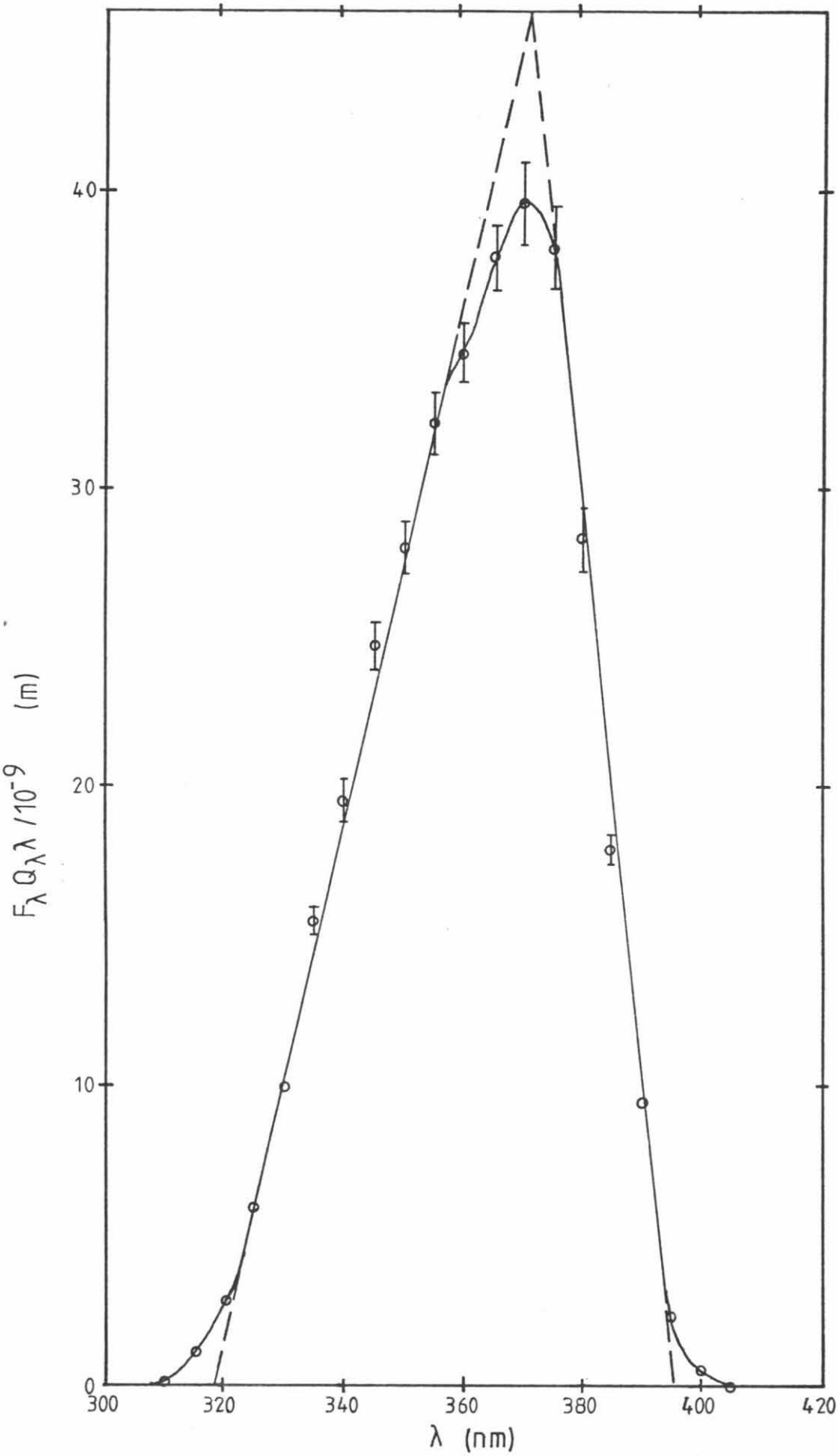

Fig: 2·3 Calculated spectral sensitivity of the UVA pyranometer.

and the irradiance $E_{UVA} = \frac{\phi_{UVA}}{A_D}$

$$= \frac{i_k}{S \; A_D} \qquad (2.4)$$

$$= (1.2 \pm 0.3) \times 10^5 \; i_k \; (Wm^{-2})$$

Experimental values of i_k yield values of E_{UVA} which are low by a factor of approximately 200. This is accounted for by the approximations used in evaluating T_D, and the true values of Q_λ being lower than those used because of the age, (many years) of the photoemissive tube used, and in assuming Q_λ to be the same as the PMT used in Chapter 3.

Electronics

The photo current is sensed by a 3140 CMOS operational amplifier wired as a current-to-voltage converter, Fig:2.1. The input impedance of the amplifier, and any variation of this, is negligible in comparison to the eighty meg-ohms resistance of the photoemissive tube. The value of the feed back resistor R sets the conversion factor of the amplifier.

$$e_o = i \; R$$

e_o: output voltage
i : detected current

The output is zeroed by a null offset potentiometer. This can be used to null the dark current signal in the output after capping the diffuser with a light stop. Alternatively if the dark current is to be monitored, the amplifier output is nulled with the input grounded across a 4.7 K resistor via switch S_1.

2.2 Cosine and linearity response

The quartz diffuser is held in place by an aluminium plate which, at low solar angles, gave reflections on to the diffuser and caused a large deviation from a flat plate response. The plate was painted matt black with a paint which has a reflectance of 6% of that of white filter paper as measured on the spectrophotometer. The resulting cosine response is shown in Fig:2.4 as

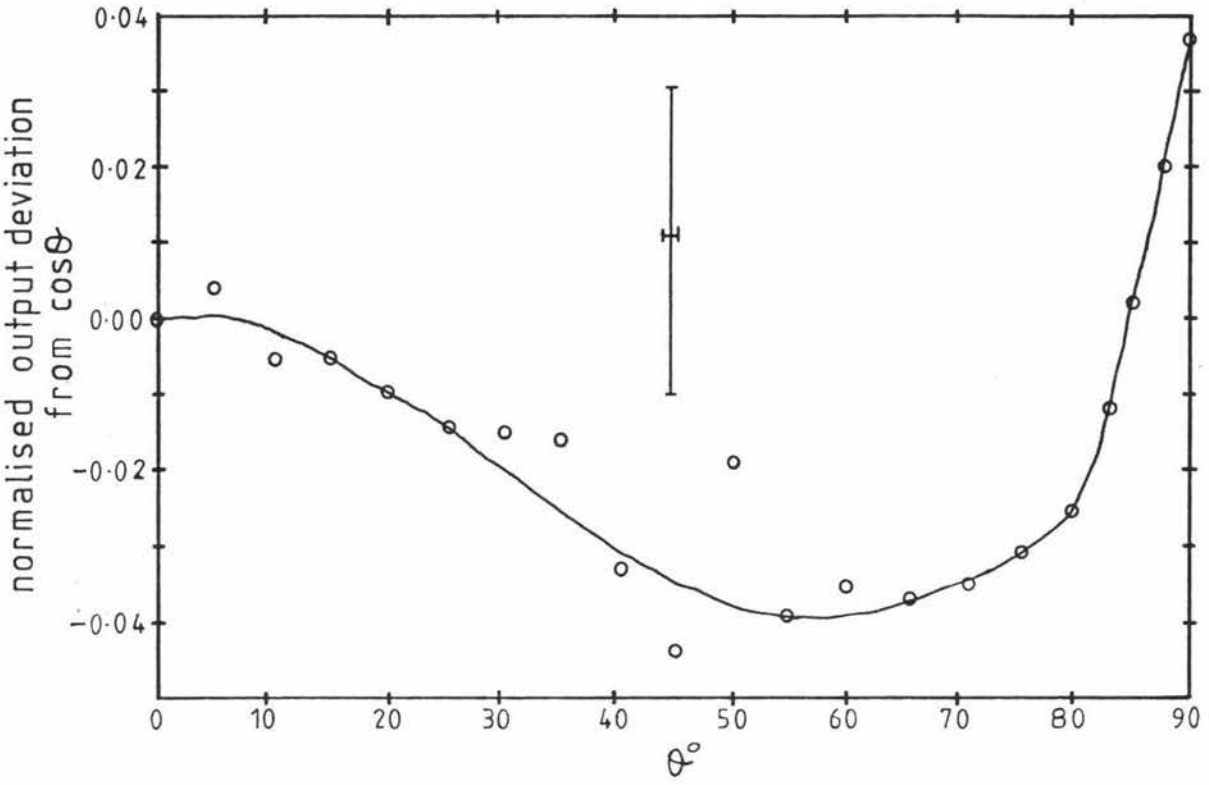

Fig:2·4 Cosine response of UVA pyranometer.

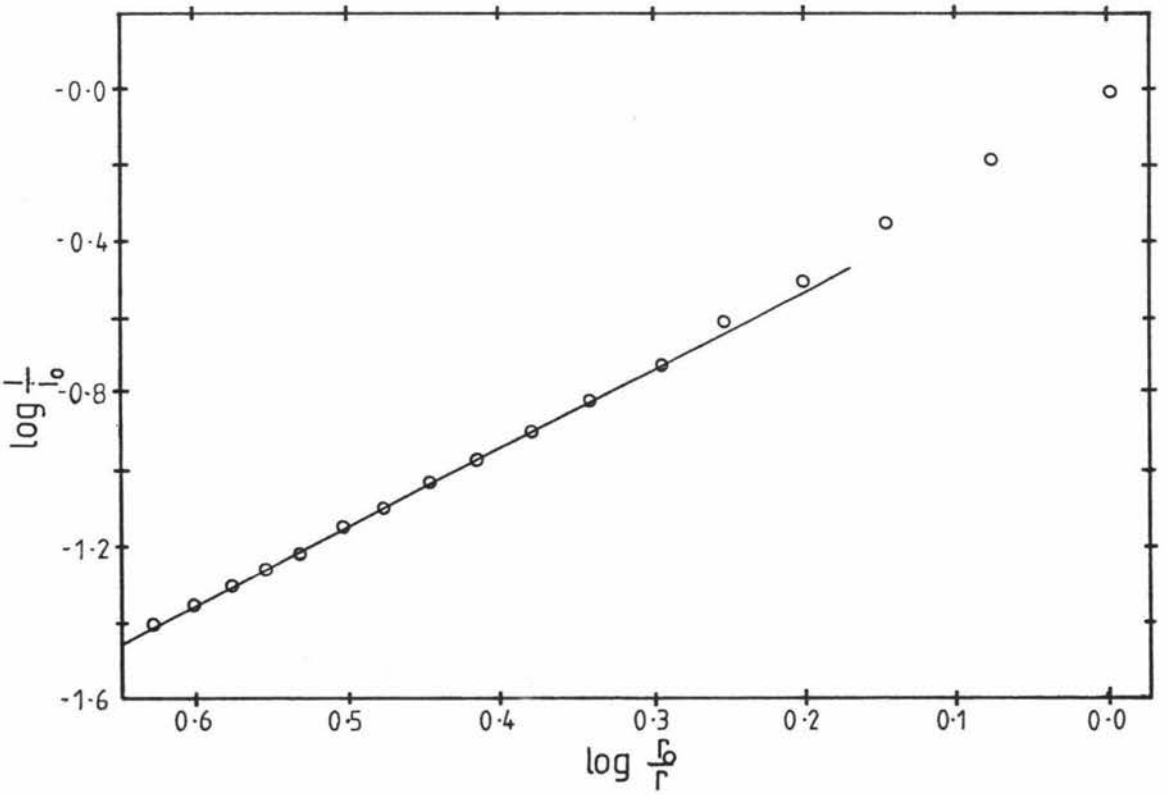

Fig:2·5 Linearity response of UVA pyranometer.

the deviation from the ideal, where the output has been normalised on the response for normal incidence. It is clear from Fig: 2.4 that the cosine response is within 5% of the ideal for all angles of incidence, and is satisfactory for the purposes of this instrument.

The output of the detector as a function of photo-cathode irradiance was checked for direct proportionality using the inverse square law to give a range of irradiances and corresponding outputs. The irradiance changes as a function of the source-detector distance (r)

as $E \propto \frac{1}{r^2}$ and if the output $\propto E$ then

$$\frac{i}{i_o} = \frac{E}{E_o} = \frac{r_o^2}{r^2}$$ where i_o, E_o, r_o are normalising factors

$$\log \frac{i}{i_o} = 2 \log \frac{r_o}{r}$$

$\log \frac{i}{i_o}$ is plotted against $\log \frac{r_o}{r}$ in Fig: 2.5. Data points in the right hand portion of the graph are ignored as the values of r for these points are less than that permissible for the inverse square law to be obeyed with a source aperture of 0.7 cm diameter. The slope of the line obtained is (2.07 ± 0.08), thus the inverse square law is obeyed and, therefore, the response of the instrument is linearly related to the incident irradiance.

2.3 Calibration

Transducer calibration can be carried out by use of a standard lamp of known spectral distribution or a light source of narrow bandwidth (of the order ofseveral nanometers) with a selectable center wavelength of emission. After scanning the active region of the transducer the calibration factor can be found by integrating over the bandwidth.

$$C = \frac{E}{I} \qquad (W\,m^{-2}A^{-1})$$

C: Calibration constant.

E: Integrated irradiance over the total bandwidth.

I: Anode current integrated over the total bandwidth.

Alternatively the value of C can be found by using a calibrated instrument of similar characteristics and exposing both instruments to the same irradiance and then using the above equation where E is

now the irradiance as measured by the calibrated instrument. Using the latter method a calibration factor was found from data obtained by running the UVA pyranometer alongside an Eppley Ultra-Violet Radiometer (No. 18183) maintained by the New Zealand Meteorological Service. The Eppley instrument has a similar spectral and cosine response [6] to the UVA pyranometer. It was last calibrated (using a standard lamp) on 13 July 1979, to an accuracy of $\pm$ 2%. Data from the two instruments was recorded on a two channel Omniscribe chart recorder over a period of two days (15,16 April 1982). This was done in order to observe any deviations between instrument responses for varying solar angles and cloud cover. Thirty five samples from the collected data were used to find the calibration factor (C) for the UVA pyranometer.

$$C = (7.2 \pm 0.4) \times 10^{7} \quad (Wm^{-2}A^{-1})$$

With this the incident irradiance (E_{UVA}) is calculated from the photo-emmisive tube anode current (I) in the following way.

$$E_{UVA} = (7.2 \pm 0.4) \times 10^{7} \; I \quad (Wm^{-2})$$

The 5% error in the value of C is comprised of, 2% accuracy of the Eppley calibration factor, 4% deviation between instrument responses with the data obtained, and a 2% error in calculating C from values read from the chart recorder.

Comparison of data collected can be seen in Fig:2.6 where the difference between the outputs, normalised at the zenith, has been plotted as a function of New Zealand standard time. It is clear on considering the size of errors in each data point that the outputs are coincident for the range of conditions under which the data was collected. It is therefore concluded that the instrument responses are coincident within the accuracy of the recorder.

2.4 Field Test results

The UVA pyranometer was run alongside a solarimeter operated by the Microclimate section of the Plant Physiology Division of the D.S.I.R., Palmerston North, for a comparison of global UVA irradiance to total global irradiance. The results are shown in Fig:2.7.

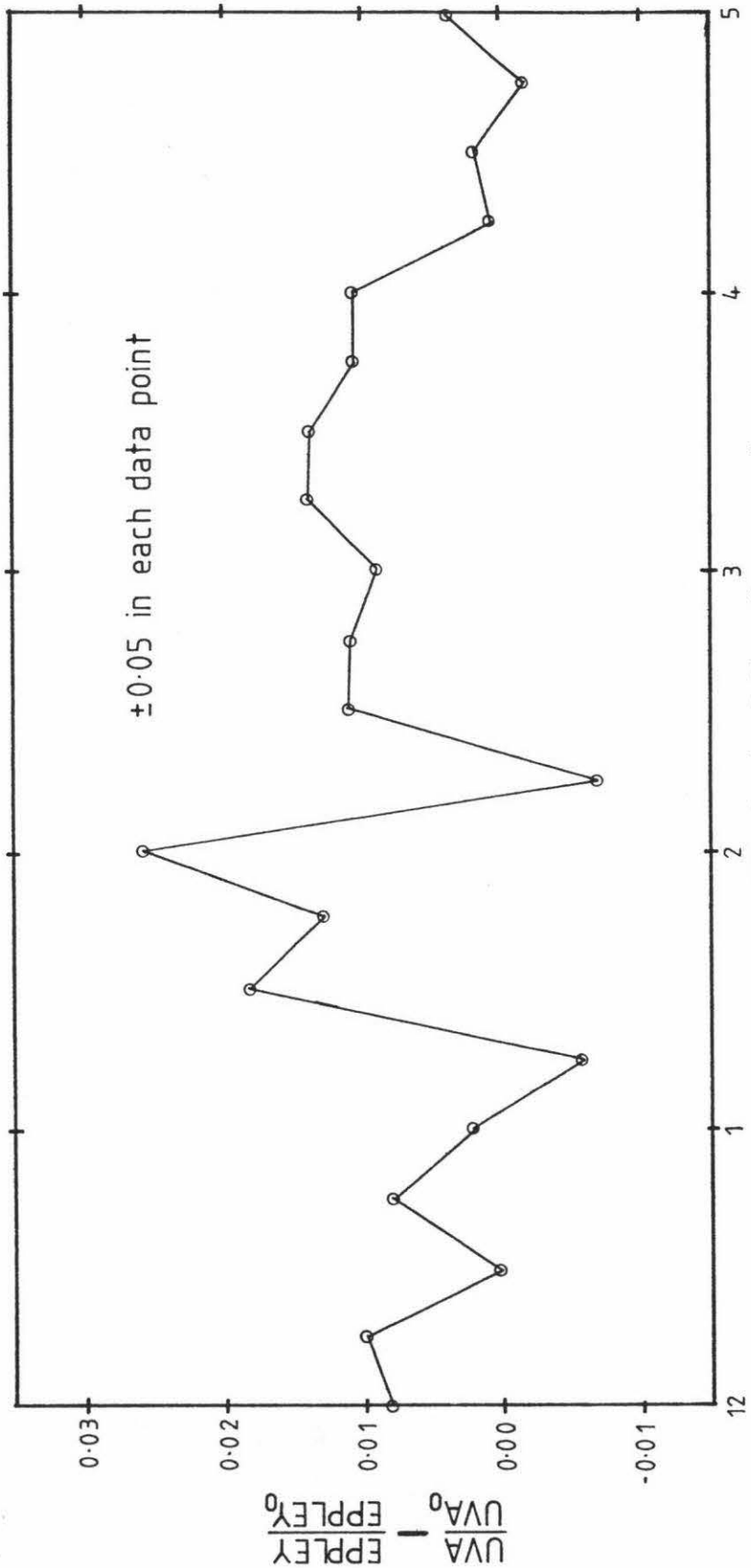

Fig :2·6 Comparism of UVA pyranometer and Eppley radiometer.

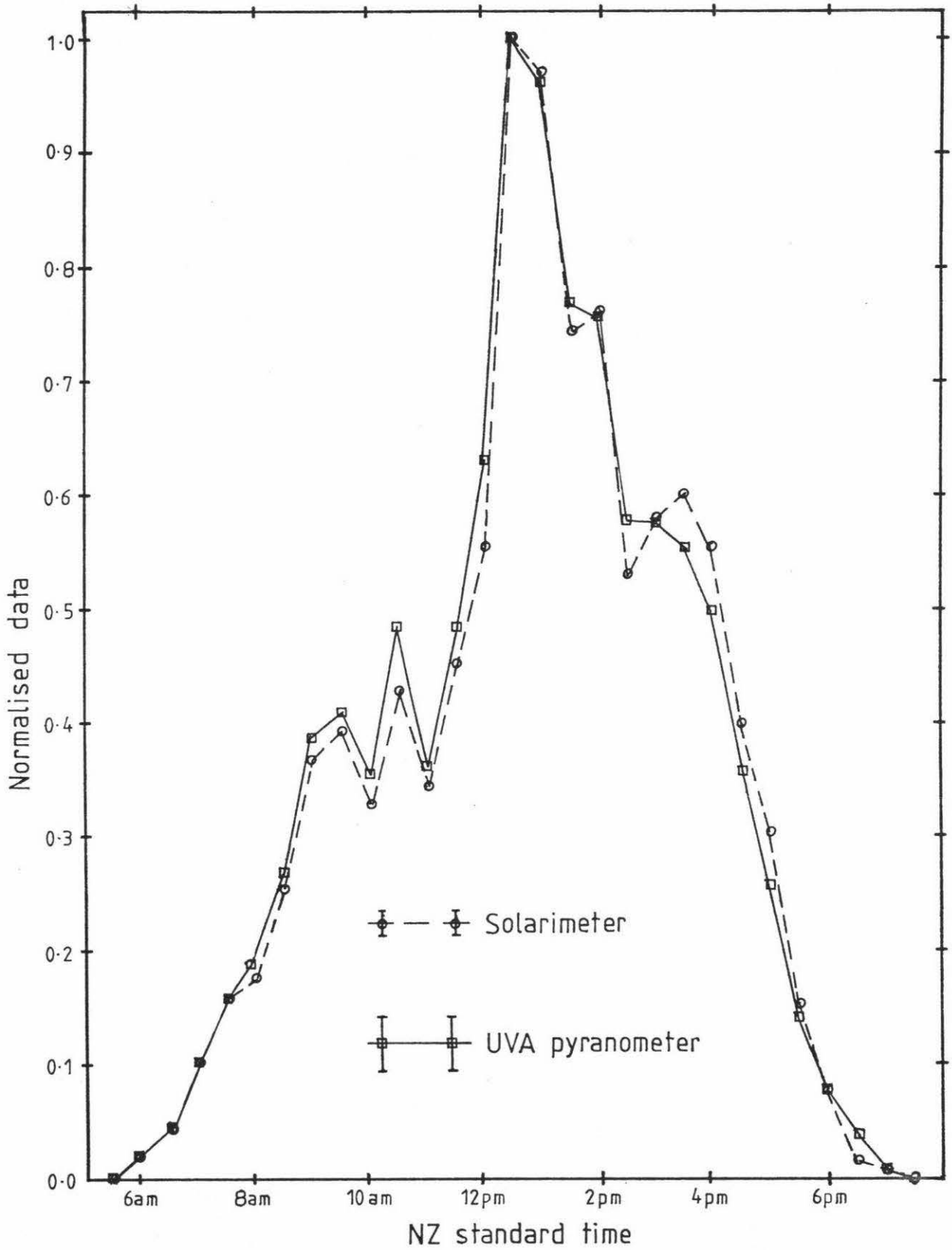

Fig:2·7 Normalised irradiance curves of global UVA and global total solar radiation, 26 October 1981.

Both sets of data are normalised on readings obtained at the solar zenith for ease of comparison. Irradiance values can be found from

$$E_{UVA} = (45 \pm 2) \text{ Normalised data } (Wm^{-2})$$
$$E_{solar} = (690 \pm 30) \text{ Normalised data } (Wm^{-2})$$

The results show that UVA irradiance is closely correlated with total irradiance. The presence of overhead cloud has contributed to the relatively low UVA afternoon readings, when a large portion of the overhead diffuse blue sky was obscured.

CHAPTER 3

UVB filter wheel Pyranometer

The primary aim of this thesis was the construction of an instrument to monitor solar UVB irradiance levels incident on a flat horizontal surface at ground level. The instrument was to be designed to conform to certain construction and operational criteria [8] .

(I) Isolation of the desired spectrum from the visible and infra-red regions is accomplished with five narrow band interference filters.

(II) The stable, sensitive detector element is a high gain EMI photomultiplier tube (PMT).

(III) Close adherence to the Lambert cosine law for a flat plate detector is achieved by the use of a diffuser as the radiation collector.

(IV) Environmental effects such as temperature and humidity can be minimised by the use of suitably protected componentry and the inclusion of hygroscopic or desiccant compounds. For increased temperature stability heaters could have been used.

(V) It is desirable, but not essential, that the instrument output be linearly related to the incident irradiance. For a Photomultiplier tube (PMT) this can be achieved by operating it at a constant voltage since the gain of the tube is a function of the applied voltage. However, for reasons which will be given later, the PMT was operated in a constant current mode. The PMT voltage is varied in order to achieve this, and, because the gain is nonlinearly related to the PMT voltage, the output is a nonlinear function of the incident irradiance. This could be linerarised with suitable electronics. However, as the instrument is designed for a routine monitoring, the output should be recorded electronically rather than by chart recorder and the linearisation of the output could then be programmed into the data-logger

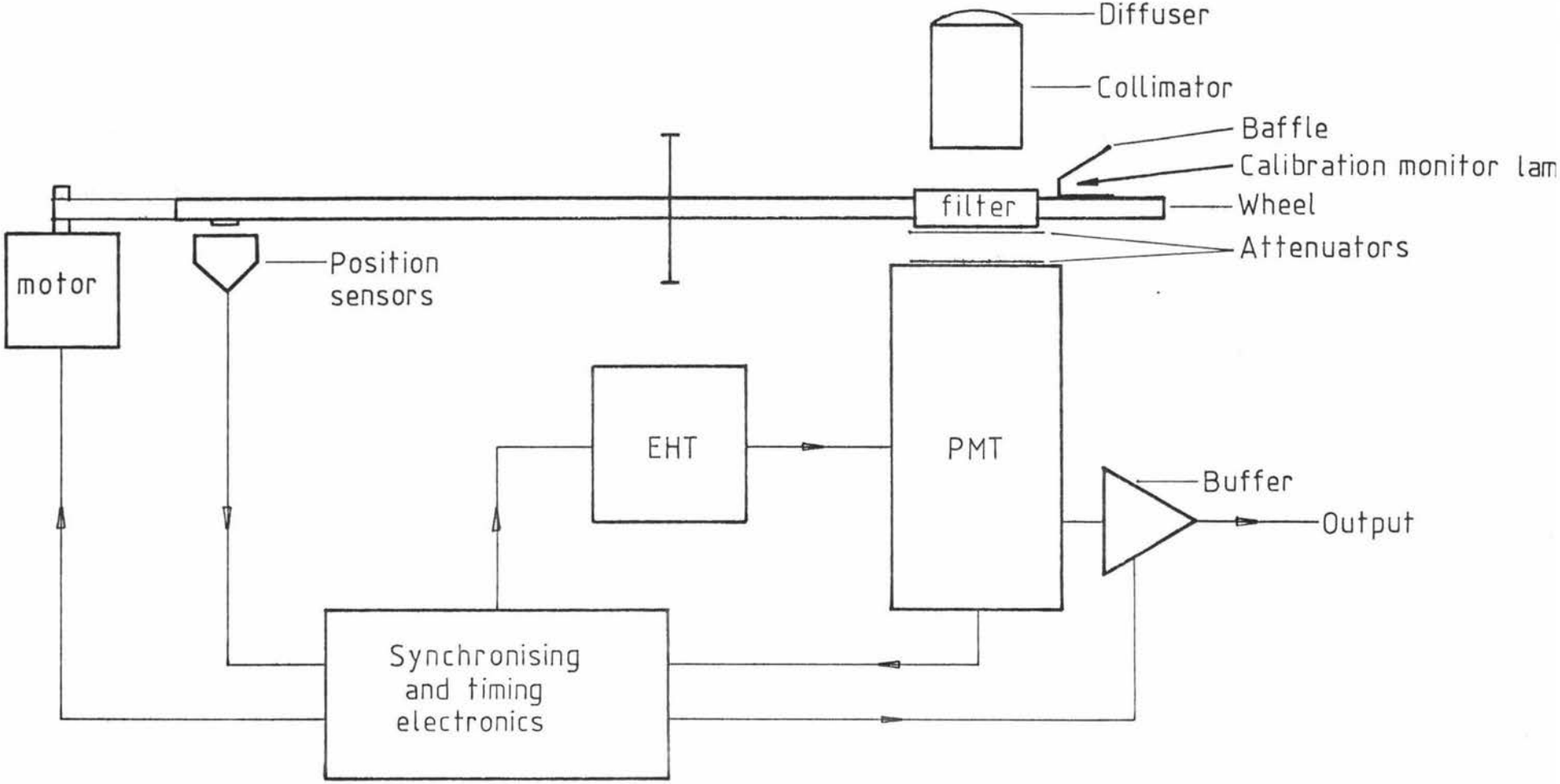

Fig :3-1 Block diagram of UVB instrument.

or the play-back data-processor.

(VI) The instrument must be simple to operate and maintain by non-specialised technicians, and also be portable and rugged for ease of transportation to remote sensing stations.

3.1 Description of the instrument.

Diffuser

Because of the unavailability of a suitably shaped diffuser of high transmittance in the UVB a sheet of "Grade 5" white filter paper moulded to the inside of a semi transparent dome was used to achieve the desired flat plate collector response. A dome of Spectrosil (fused quartz) that has high transmittance to the UVB is required for spectral measurements below approximately 295 nm. The raising of the flat plate diffuser into a dome shape enhances the Lambert Cosine law response for low solar angles [6].

Collimator

The collimator is required to keep the angle of incidence of radiation on to the surface of the interference filters within certain limits. Deviations outside these limits will cause a shift in the filter pass band [9]. Schott product information [10] indicates that apertures up to $\theta=20^{o}$ at normal incidence give variations of no practical importance. Fig : 3.2 shows the construction dimensions used to achieve this.

The collimator design includes three light baffles to stop any reflected radiation from the collimator walls reaching the PMT photo cathode. The collimator is also painted with matt black paint of reflectance 6% (see Chapter 2) to further reduce the effects of reflected radiation. As in Chapter 2 the diffuser and collimator together act as a neutral density filter and from equation (2.1) in Chapter 2 the effective transmittance (T) is given by

$$T = \frac{A_D}{A_{aperture}} \frac{\Omega}{4\pi}$$

$$= (9\pm1) \times 10^{-3}$$

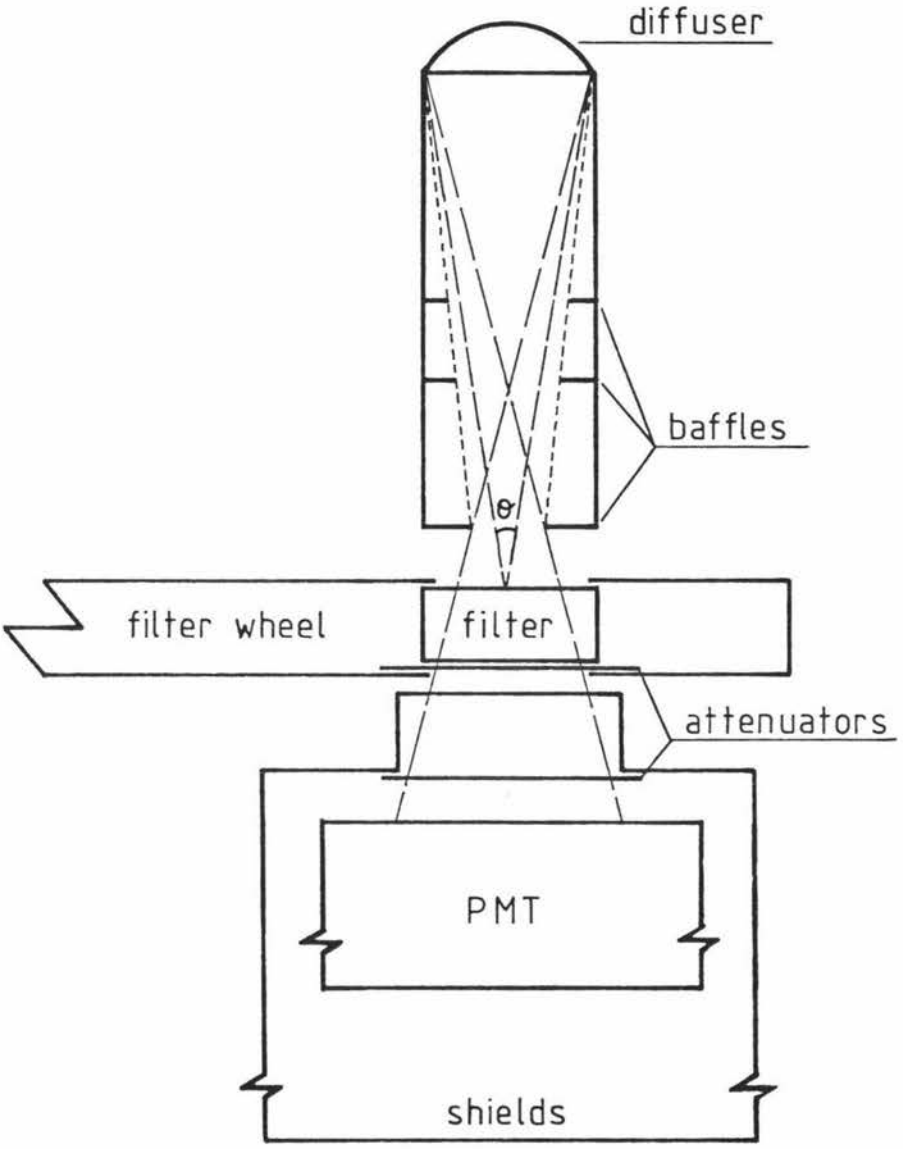

SCALE 1:1

Fig:3·2 Collimator,filter and PMT alignment.

This transmittance does not include the spectral transmittance, D_λ, of the protective dome, Fig: 3.3.

Filters

Interference filters with band widths of approximately 10 nm were used, as fine structure information is not required and the solar spectrum is considered as smooth over this interval [6]. The five filters used have peak transmittance values at the approximate wavelengths 280, 290, 300, 310, 320 nm, and the spectral transmittance curves are shown in Fig: 3.4. An expanded transmittance scale is used to obtain the out-of-main-passband measurements more accurately as shown in Fig: 3.5. This accuracy is required because the solar irradiance changes by a factor of approximately 10^{10} over the wavelength range 285 to 300 nm, with the result that irradiance passed by the long wavelength skirts of the 280, 290 and 300 nm filters is comparable in magnitude to that passed by the main passband. Data from Robinson [1] shown in Fig:3.6 illustrate this.

The variation of interference filter transmittance characteristics with temperature [11] are negligible, over a range of 0 to 40°C in comparison to overall instrument accuracies (Section 3.6). The variation of transmittance across the surface of the filters, as well as changes in sensitivity across the photocathode of the PMT, are minimised by synchronising the filter wheel sampling position with the collimator and photo cathode position. In this way the previously calibrated sections of filter and photocathode (Section 3.6), are used for each sample. Dependence of transmission factor on the angle of incident irradiance has been minimised as described previously. Ageing of interference filters is primarily caused by the absorption of moisture, and causes a shift to longer wavelengths of the spectral transmittance in the order 0.1 to 2% immediately after manufacture [11], and lesser amounts after that. The use of humidity proofed filters, and a desiccant in the instrument reduce the uncertainty in the central transmittance wavelength to 0.01 nm.

For the purpose of comparison a section of the visible spectrum near the peak wavelength of the solar irradiance spectrum was also monitored using a combination of two Ilford gelatin filters. The transmittance spectrum of the filters when overlapped gave the desired passband and low transmittance required to attenuate the irradiance levels to within the design limits of the PMT. The two filters used

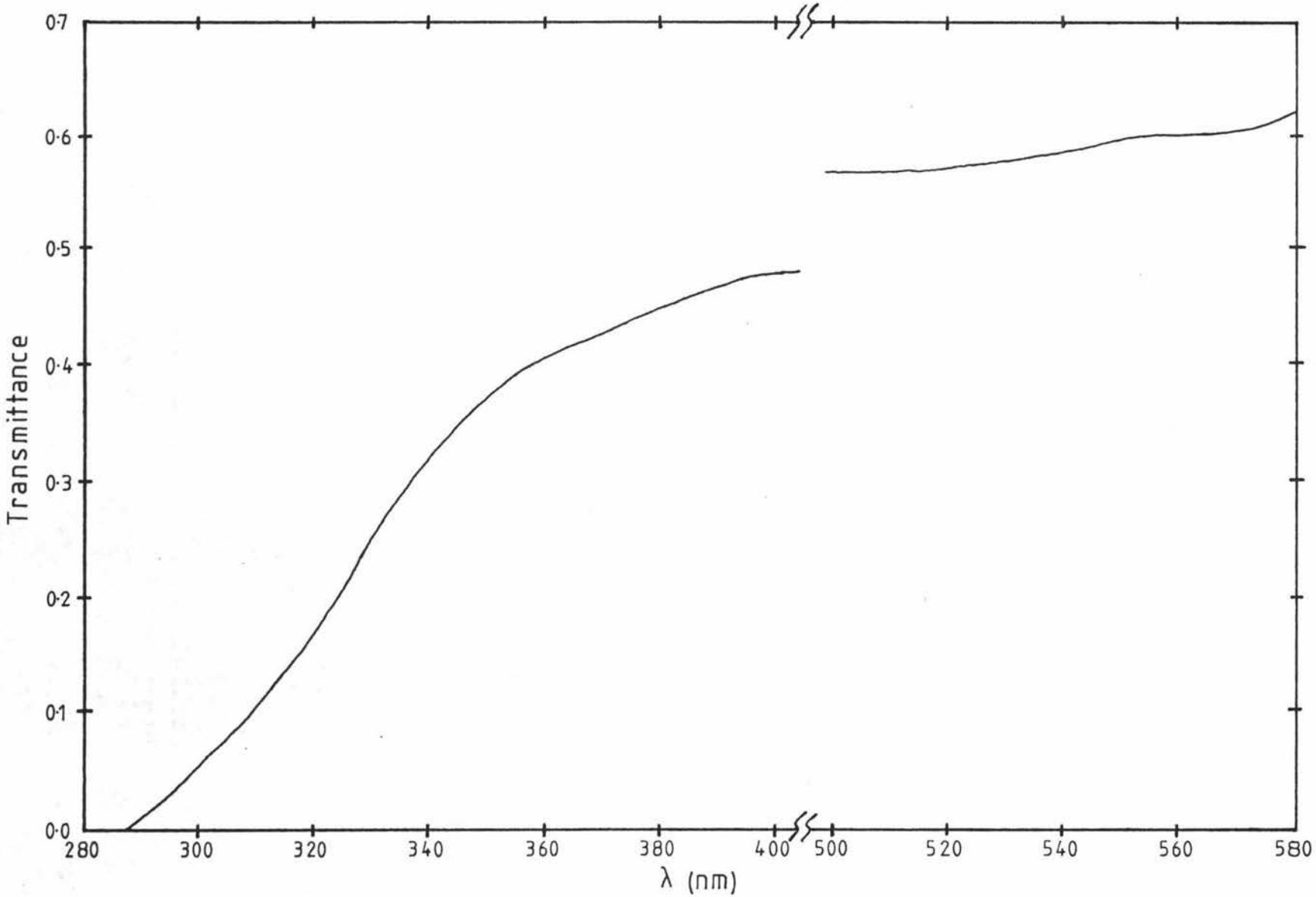

Fig:3·3 Protective dome spectral transmittance.

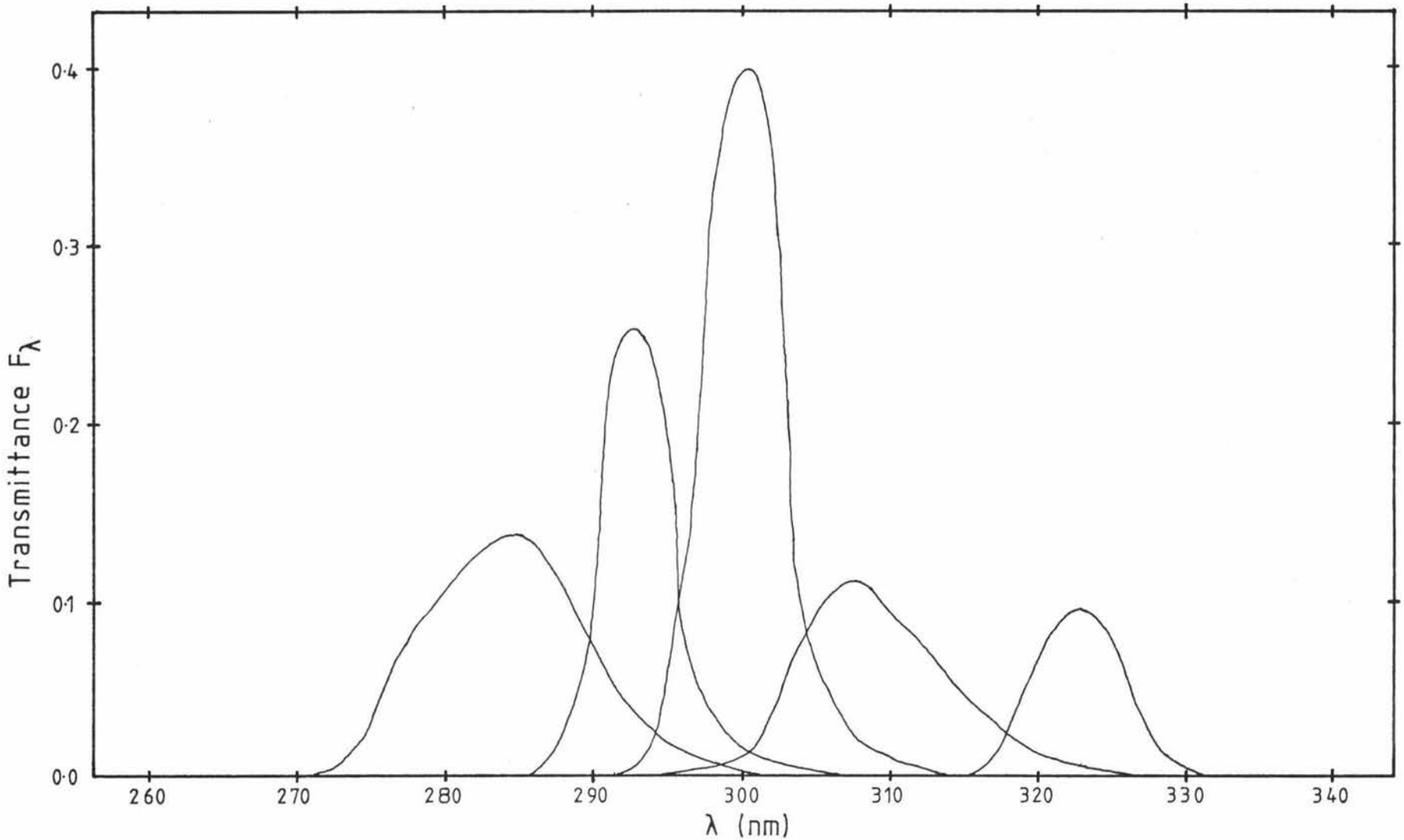

Fig :3·4 UVB interference filter spectral transmittance curves.

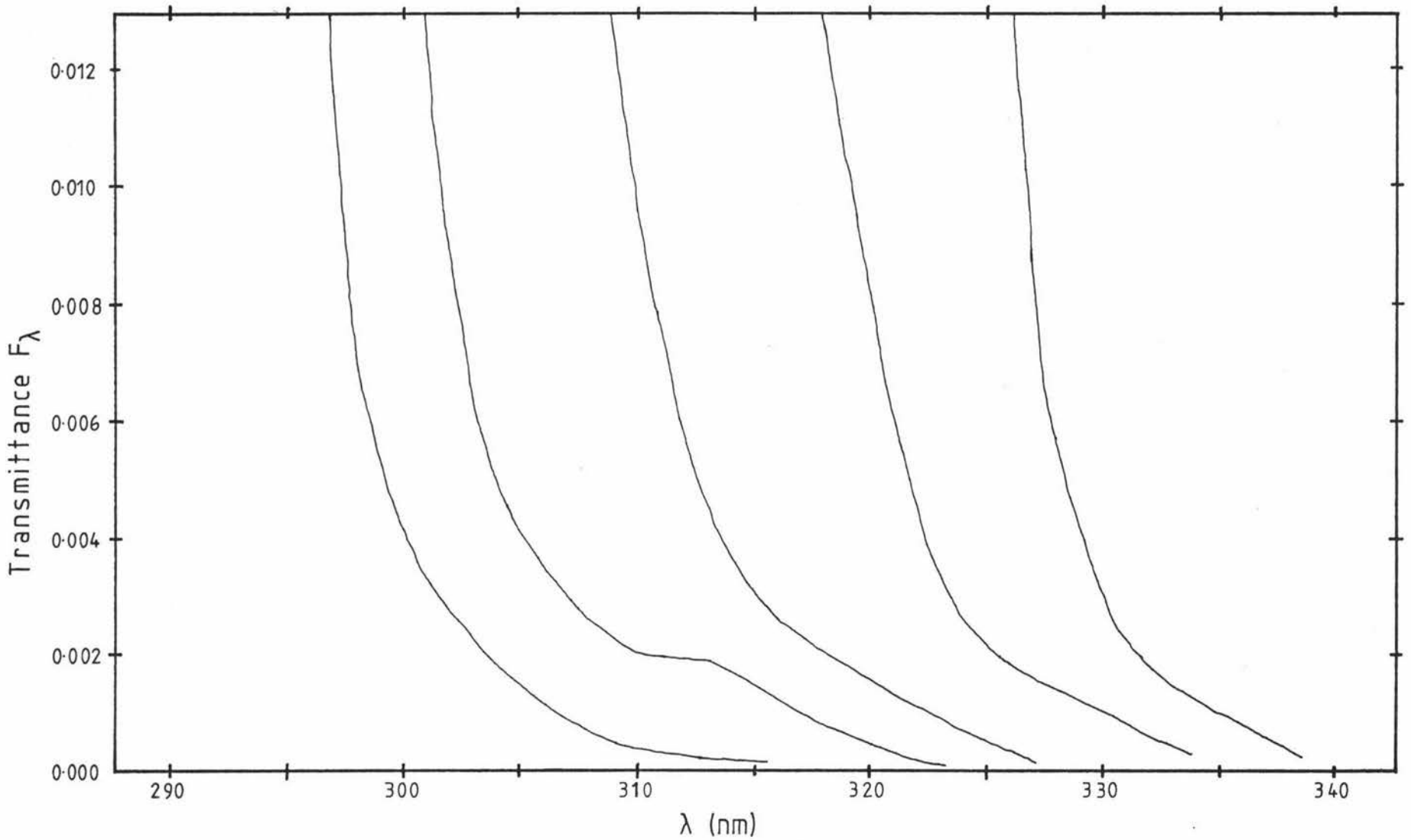

Fig:3·5 Upper cut-off transmittance curves of UVB interference filters.

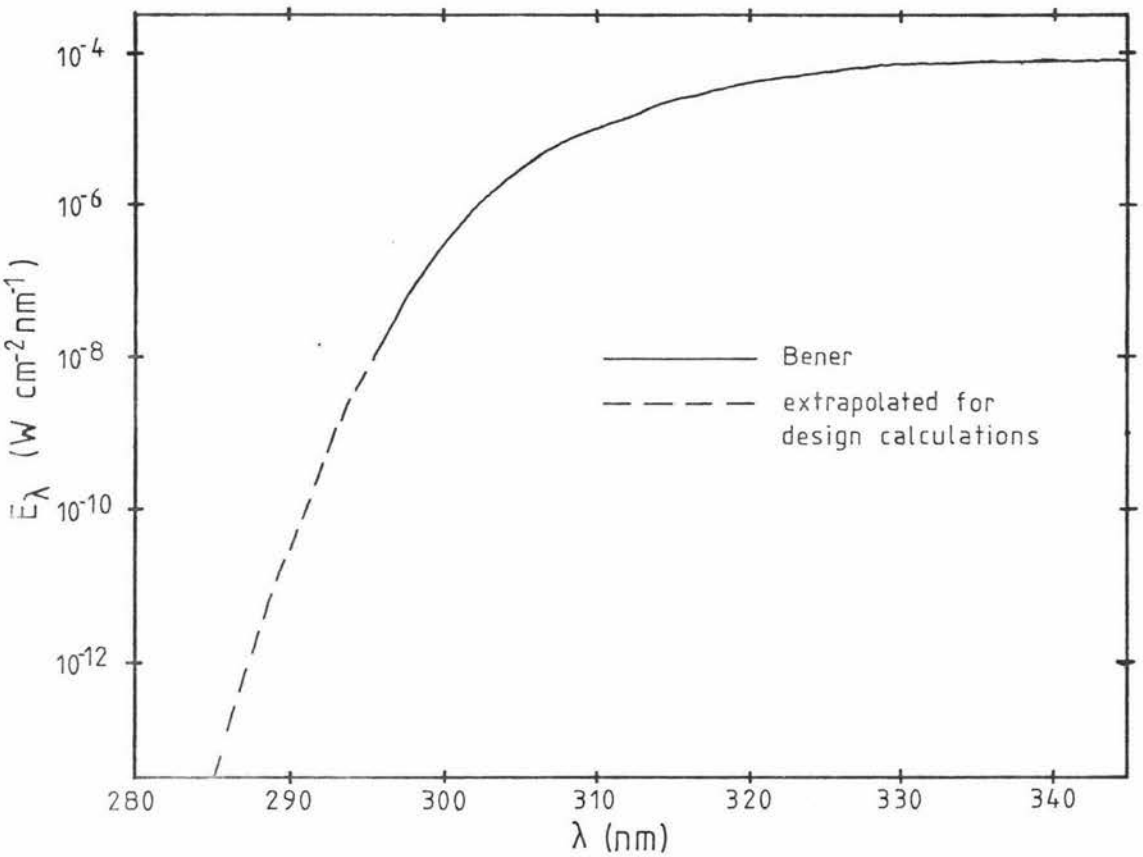

Fig:3·6 Data by Bener from Robinson [1], for a solar angle of 50° at Davos-Platz, Switzerland.

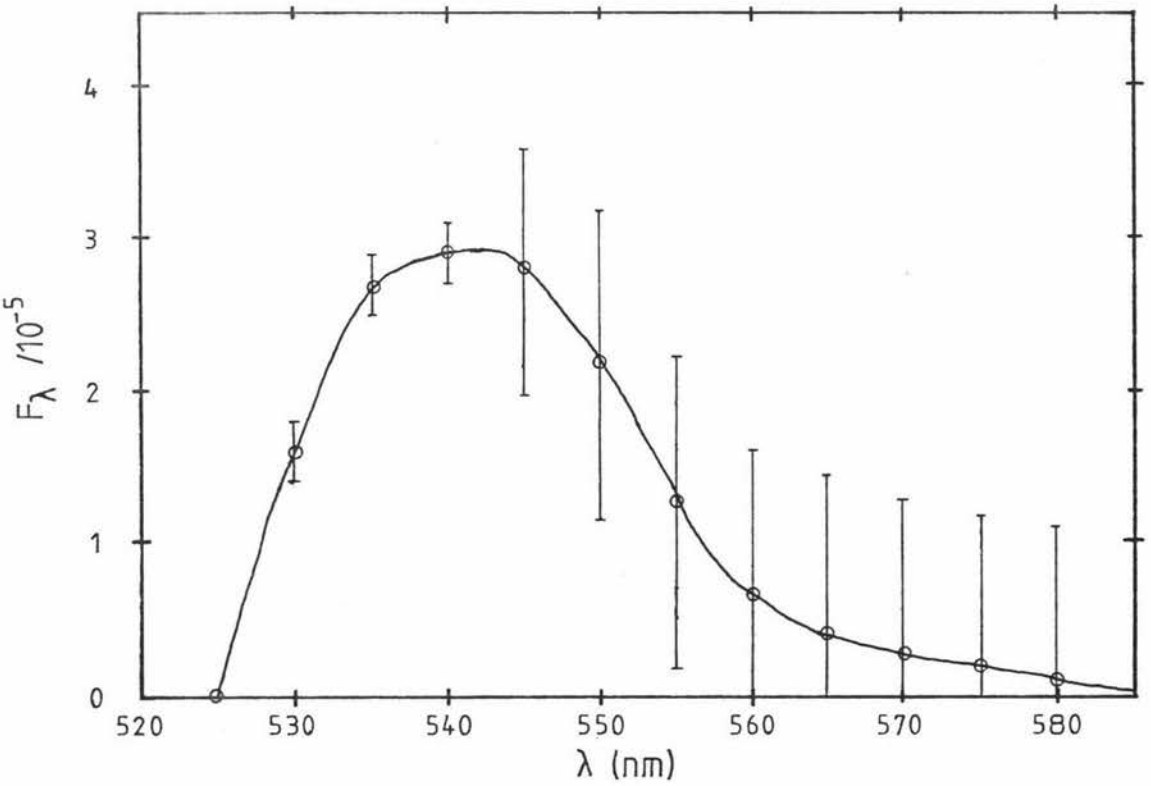

Fig:3·7 Calculated visible filter spectral transmittance.

were numbers 603 (spectrum blue-green) and 604 (spectrum green) with the resultant spectral transmittance shown in Fig: 3.7.

Attenuators

The large range of incident irradiances over the UVB spectrum is beyond the sensitivity range of the PMT detector. To prevent the irradiance of the PMT cathode from exceeding manufacturers' specifications, the incoming beam is attenuated when the appropriate filters are above the PMT cathode. The attenuators used are stainless steel gauzes as for the UVA pyranometer in Chapter 2. Each gauze has a transmittance of 0.39 which was constant over the entire spectral region of interest. Measurements of different portions of the gauze indicate an uncertainty of $\pm 10\%$ in the Transmittance Value. Where more than one attenuator was required every second gauze was orientated so that the gauze mesh is 45^{o} from that of the adjacent gauze. This is to minimise any overlapping effects of the gauze mesh. If more than three gauzes were required they were separated into groups of three or fewer and separated by at least one centimeter to avoid focussing effects from Moire' fringes. The gauze attenuators were positioned between the filters and the PMT cathode because of filter transmittance dependence on the angle of the incident radiation.

Calibration Monitor

Over periods of time PMT detectors lose sensitivity and the calibration constants require re-evaluating [12]. To indicate deviations of PMT sensitivity a reference light source is sampled once each filter wheel revolution. The tungsten filament light source is mounted in a collimating tube and the beam directed parallel to the plane of the filter wheel. When sampled the beam is diffusely reflected down through the filter wheel onto the PMT photo cathode. Light baffles are rotated in front of the constant light source to reduce stray light when other channels are sampled. To achieve a constant light source free of fluctuations the light bulb is operated at constant d.c. voltage. Standard burning-in procedure was used i.e. the 6 volt tungsten filament bulb was operated at an over voltage of 8 volts for several hours, and then

operated at a working voltage of 2,8 volts, being several volts under the normal working voltage as required for stable operation.

Photomultiplier tube detector

A detector that had the required high gain, spectral sensitivity, and was available in the department, was an EMI type 9656 QB PMT. Specifications are given in appendix II. The PMT is operated with the overall voltage controlled by a feedback circuit that keeps the anode current constant. It is so operated because of fatiguing of the dynodes and space charge saturation effects at the last dynode when the PMT is continuously operated at high voltages. The high voltage supply is also turned off between sample periods to further reduce these problems. The gain of the PMT is a power law function of the applied voltage, and the range of detectable incident irradiances is therefore greatly extended by using the varying voltage instead of the constant voltage mode of operation. The constant voltage mode has an approximate 10^2-fold range and the constant anode current mode has an approximate 10^4-fold range. When operating at high gains the PMT is susceptible to interference from magnetic and electrostatic fields. A mu-metal shield and a galvanised steel enclosure were used to eliminate this interference. Except for an aperture over the photocathode, the galvanised steel envelope is of light-tight construction.

3.2 Calculation of attenuation factors.

The manufacturer's operational constraint of a maximum photo cathode current density of 0.02 $\mu A/cm^2$ is used in determining the maximum allowable incident irradiance. The sensitivity of the photo cathode is found from equation(2.2)in Chapter 2.

$$s_\lambda = \frac{i_k}{\phi_\lambda}$$

$$= 8.065 \times 10^5 \lambda Q_\lambda (A\ W^{-1}\ nm^{-1})$$

The quantum efficiency, Q_λ, as given by the PMT manufacturer is shown in Fig: 2.2, and values of s_λ are shown in Fig: 3.8.

The value of s_λ for the visible filter is considered, for further calculations, to be constant at the calculated value, at λ=540nm, of $s_\lambda=(3.92\pm0.05)\times10^{-2}$ A $W^{-1}nm^{-1}$.

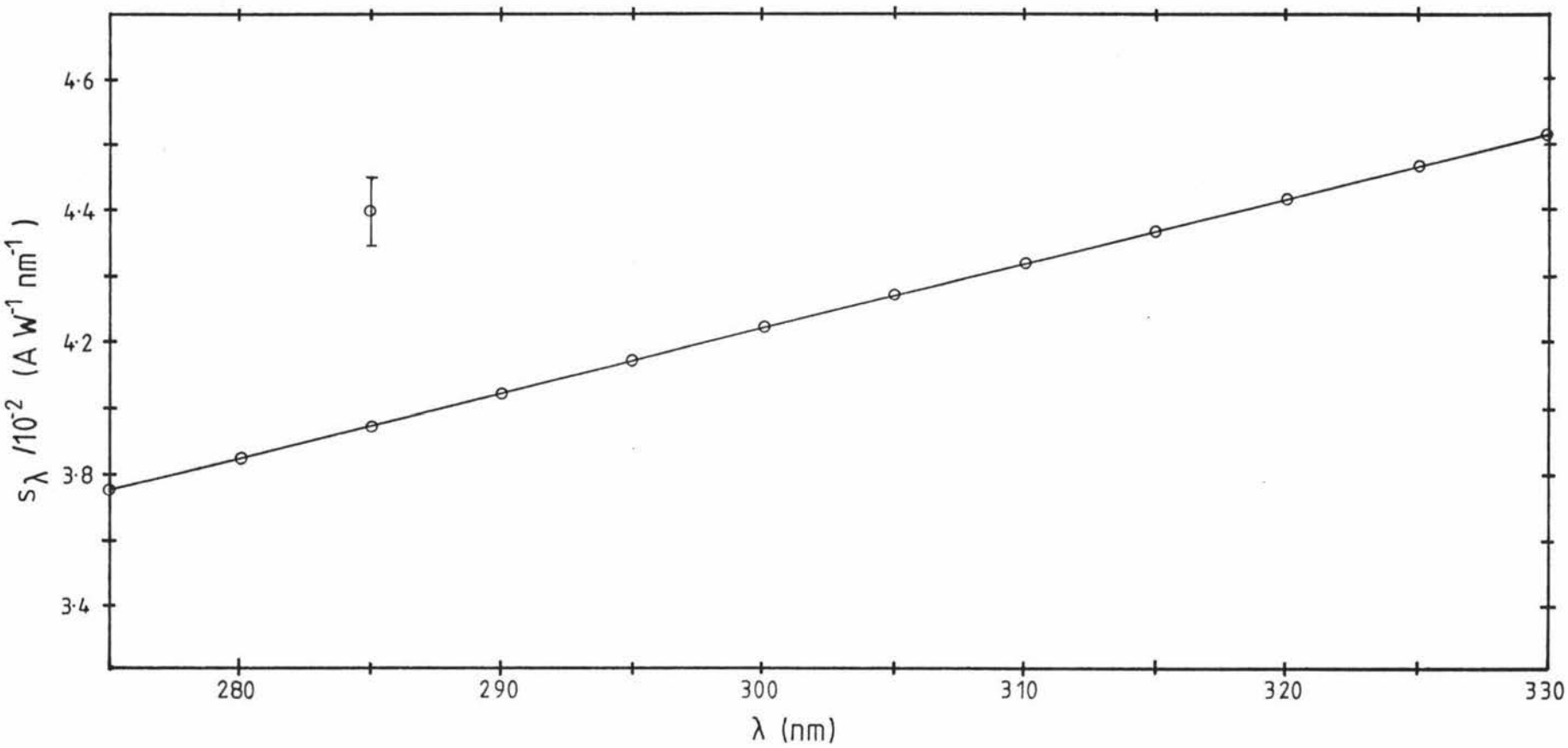

Fig :3·8 Calculated photocathode sensitivity.

The maximum irradiance allowable on the photo cathode is found from the expression

$$E_{\lambda,k,max} = \frac{\phi_{\lambda,k,max}}{A_K}$$

$$\phi_{\lambda,k,max} = \frac{i_{k,max}}{s_\lambda}$$

$$i_{k,max} = 0.02\times10^{-6} A_K \ (A)$$

thus $$E_{\lambda,k,max} = \frac{0.02\times10^{-6}}{s_\lambda} \ (W cm^{-2})$$

and $$E_{k,max} = \int_{\lambda_1}^{\lambda_2} E_{\lambda,K,max} \, d\lambda$$

$$= 0.02\times10^{-6} [\int_{\lambda_1}^{\lambda_2} s_\lambda \, d\lambda]^{-1} \quad (3.1)$$

The bandwidth for each integration is found by considering the transmitted irradiance of each filter for the maximum expected incident spectral irradiance at the instrument. An approximation of the maximum spectral incident irradiance can be made with data from Fig:3.6. To correct for the solar angle not being 90^o an increase by a factor of approximately 1.3 is required. This factor is found using an extinction coefficient of a=0.18 [1] in equation (1.1) in Chapter 1.

The transmitted irradiance spectrum is found from the following expression.

$$E_{\lambda,k,max} = E_{o\lambda,max} \, 1.3 \, T \, D_\lambda \, F_\lambda$$

Eo_λ : incident spectral irradiance and $E_{\lambda,k}$ the transmitted spectral irradiance to the photo cathode.
The results can be seen in Fig: 3.9 and Fig: 3.10.

For the visible filter the incident irradiance and dome transmittance can be approximated as constant and therefore the bandwidth limits can be found from Fig: 3.7. The band width is specified by the wavelengths at which the transmittance is half the maximum transmittance value. However for the UVB interference filters the irradiance values change rapidly with wavelength as

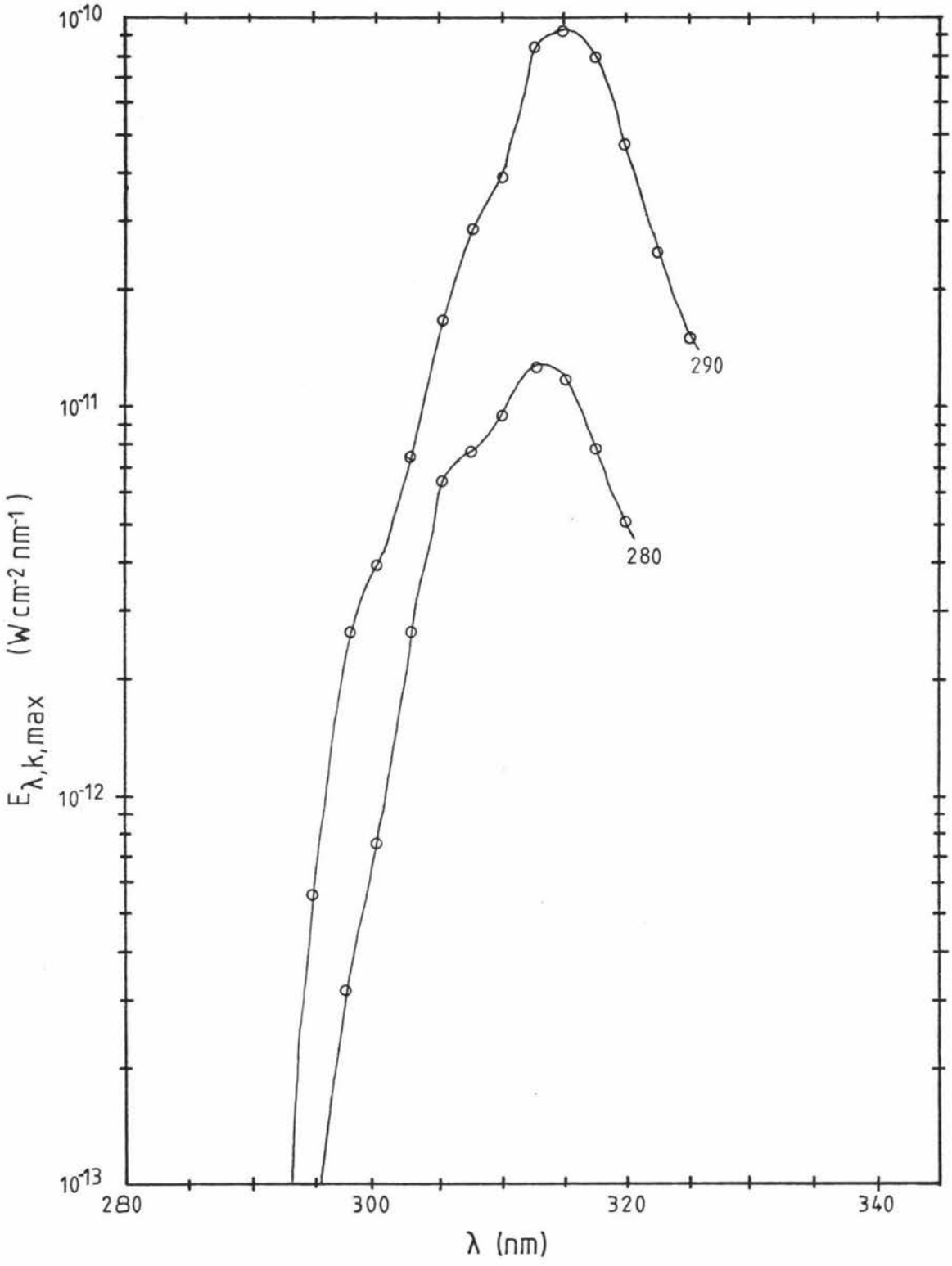

Fig:3·9 Calculated spectral irradiance transmitted by interference filters.

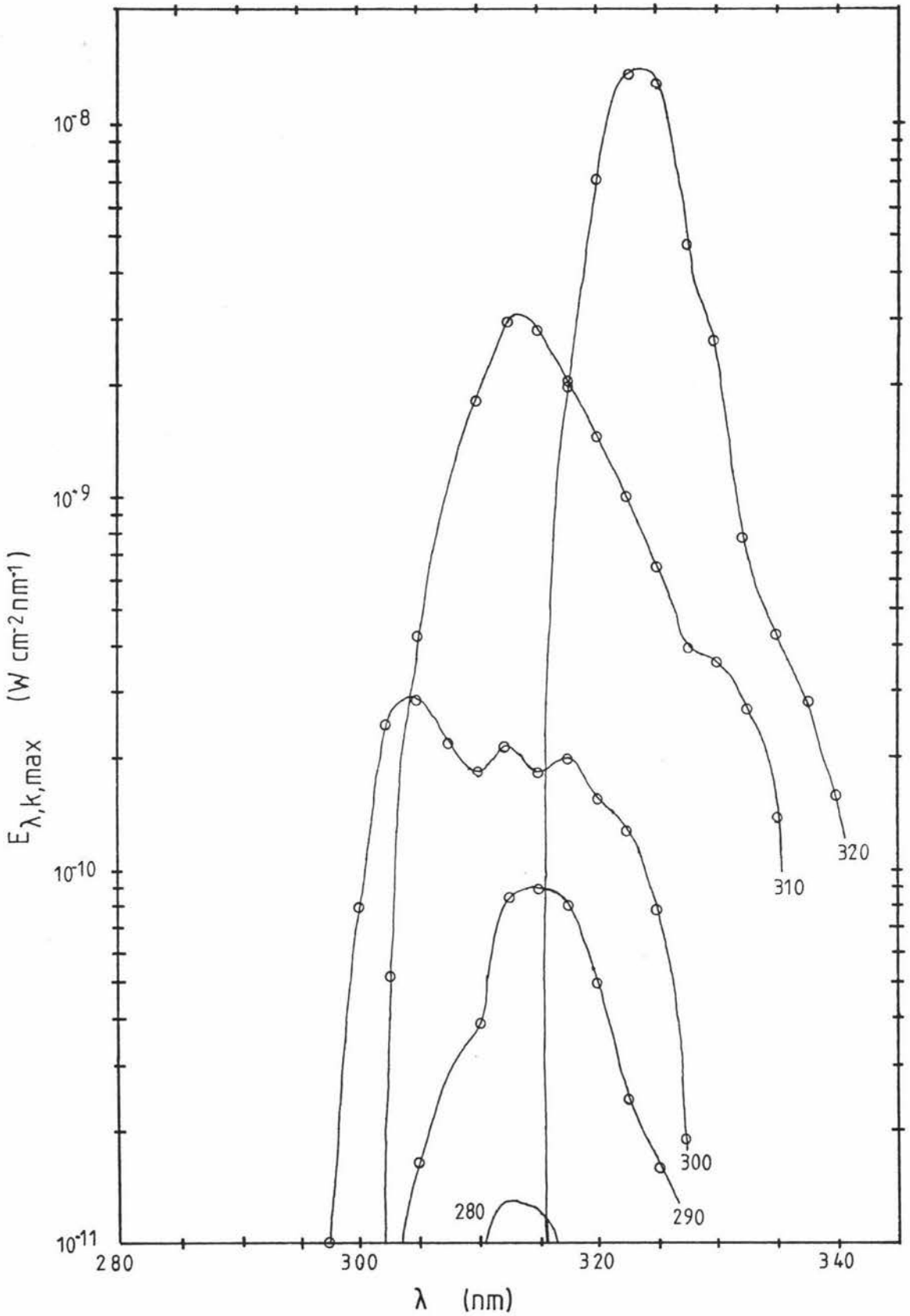

Fig :3·10 Calculated spectral irradiance transmitted by interference filters.

shown in Fig: 3.6, and this causes the transmitted spectrum to differ from the filter transmittance spectrum. The bandwidth limits are determined, therefore, by considering the wavelengths for which the transmitted irradiance is at half the maximum value. The bandwidth limits are given in Table II.

Table II: Transmitted irradiance spectral charateristics of UVB instrument filters

Filter	λ_1(nm) ±0.3	λ_2(nm) ±0.3	Bandwidth=$\lambda_2-\lambda_1$(nm) ±0.4
280 nm	305	318	13
290 nm	310	320	10
300 nm	302	318	16
310 nm	310	318	8
320 nm	320	327	7
Visible	528.5	554.5	26

From equation 3.1 and Fig: 3.8 and using the above bandwidths, the approximate maximum allowable irradiance levels at the photo cathode were calculated for each filter and are given in table III.

Table III: Maximum allowable irradiance levels at the photo cathode

Filter Channel	$E_{k,max}$ / 10^{-8} (Wcm^{-2})
280 nm	3.4
290 nm	4.4
300 nm	2.8
310 nm	5.5
320 nm	6.1
Visible	2.0

The predicted maximum irradiance of the photo cathode is found from Fig: 3.9 and Fig: 3.10 as the integral over the total passband, of the spectral irradiances transmitted by each filter

$$E_{k,max.predicted} = \int_{\lambda_1}^{\lambda_2} E_{\lambda,k,max.\ predicted}\, d\lambda$$

The results are shown in Table IV.

Table IV: Calculated maximum irradiance levels for UVB instrument

Filter Channel	$E_{k,max.\ predicted}/10^{-8}$ Wcm^{-2}
280 nm	0.13
290 nm	0.68
300 nm	3.5
310 nm	12
320 nm	68
Visible	0.10

Where $E_{k,max.\ predicted}$ for the visible filter is 3.8×10^{-11} $Wcm^{-2}nm^{-1}$. From these results it was predicted that the attenuators would be required for the 300, 310 and 320 nm filters. However experimental results showed that the attenuators given in table V were required.

Table V: Attenuators required for UVB filter channels

Filter Channel	Gauze attenuators Required.	Total Attenuator Transmittance.
280 nm	4	0.022
290 nm	2	0.150
300 nm	5	0.009
310 nm	3	0.058
320 nm	4	0.022
Visible	0	1.000

To avoid Moiré fringe effects and to minimise the number of gauzes required two gauzes were mounted on the PMT steel envelope, and the remaining gauzes were mounted on the filter wheel below each filter. As a consequence the visible filter also has an attenuator which has to be allowed for in later analysis.

Explanation of the under estimation of attenuation required is attributed to two main sources. The first is the calculation of the collimator and diffuser transmittance and the large errors associated with the approximations used. The main contributing factor is the low rejection of unwanted radiation outside the main passband of each filter. This is most prevalent in the 280, 290 and 300 nm filter passbands and is clearly illustrated in Figs: 3.9 and 3.10 as a shift in the transmitted passband compared to the filter passband. Also an out-of-main-passband peak was later located while calibrating

the instrument, section 3.6, and is discussed later.

3.3 Overall PMT Sensitivity

The Manufacturer's specifications provide sensitivity data in units of Amps per Lumen (A lm^{-1}) which are unsuitable for use in the UV and not easily converted to the units required of Amps per (Watt - nanometer) (A $W^{-1}nm^{-1}$). The PMT sensitivity can, however, be calculated from the expression

$$S = \frac{I_{\lambda,A}}{\phi_K} \qquad (3.2)$$

$$I_{\lambda,A} = G\ i_{\lambda,K}$$

$$G = \frac{M}{S} \times 10^6$$

$$S_\lambda = \frac{M}{S}\ s_{\lambda,k} \times 10^6 \quad (A\ W^{-1}nm^{-1}) \qquad (3.3)$$

G : gain of PMT in A lm^{-1}.

S_λ : total PMT sensitivity as a function of wavelength and gain.

$I_{\lambda,A}$: PMT anode current in Amps per nanometer for irradiance in Watts per (meter ^{2}nm) at wavelength λ, of the photo cathode.

s : Photo cathode sensitivity in μA lm^{-1}.

The gain of the PMT is a Power Law function of the applied high voltage, and the sensitivity can, therefore, be found as some function of the overall applied voltage. Using the manufacturer's calibration factor of s = 98 μA lm^{-1}, at an overall PMT voltage of 1110 volts, and data from Fig: 3.8 and appendix II, the data for Fig: 3.11 was calculated from equation 3.3 for a wavelength of λ=300nm. It was found upon calculation that the sensitivity vs voltage curves for the peak transmittance wavelength for each filter can be considered equivalent within the errors shown and, therefore, all further calculations will assume no wavelength dependence of S between filters. The expression for the curve in Fig: 3.11 is of the form $S = a\ V^b$ where $V = \frac{V_{EHT}}{500}$

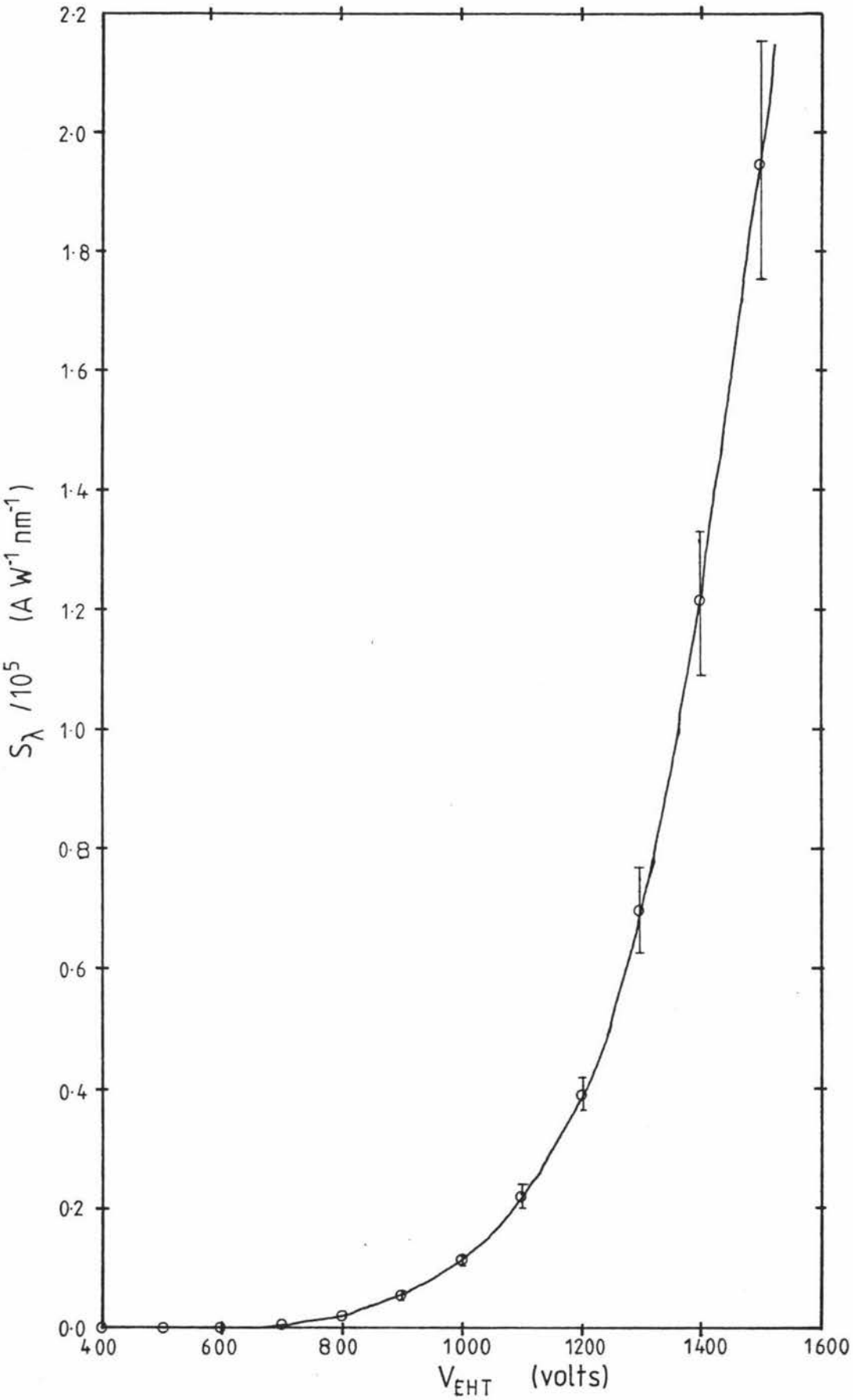

Fig:3·11 Overall PMT sensitivity as a function of applied voltage.

and S is the spectral sensitivity of the PMT for all filter channels. The reason for dividing V_{EHT} by 500 is explained later. After normalising and taking logarithms the expression takes the form $\log(\frac{S}{S_o}) = \log a + b \log V$.

Where $S_o = 30.4\ A\ W^{-1}nm^{-1}$ and S_o and V_o correspond to the maximum photo-cathode irradiance. The resulting data is plotted in Fig: 3.12 and the curve is approximated by two linear expressions. Using linear regression techniques the equations for the straight lines were found. The resulting expressions for S are,

$$\text{for } V < (1.7\pm0.3)\ \text{Volts} \quad , \quad S = (31.6\pm0.3)\ V^{(8.8\pm0.2)}\ (AW^{-1}nm^{-1})$$

$$\text{for } V \geqslant (1.7\pm0.3)\ \text{Volts} \quad , \quad S = (70\pm10)\ V^{(7.24\pm0.08)}\ (AW^{-1}nm^{-1})$$

where the conditions on V are found from the intersection of the two expressions. The irradiance of the photo cathode (E_k) as a function of the applied voltage can now be found using equation (3.2) to obtain

$$E_k = \frac{I_A\ \Delta F}{s\ A_k}$$

ΔF is the effective bandwidth of each filter from table I.

Thus, for $V < 1.7$ Volts, $$E_K = \frac{I_A \Delta F}{A_K} (3.16 \pm 0.03)10^{-2}\ V^{-(8.8\pm0.2)} \qquad (3.4)$$

for $V \geqslant 1.7$ Volts, $$E_K = \frac{I_A \Delta F}{A_K} (1.4 \pm 0.2)\times10^{-2}\ V^{-(7.24\pm0.08)} \qquad (3.5)$$

To obtain the greatest sensitivity when operating at the maximum PMT Voltage, the anode current should be at the minimum value usable. This minimum is limited by the dark current of the PMT and with a PMT Voltage of 1450 V the dark current is typically 20 nA. Thus a value of $I_A = 0.2\mu A$ was chosen as a compromise between high sensitivity and a 10% dark current value that has to be compensated for. This value of I_A is 3 orders of magnitude less than the maximum allowable.

PMT over exposure protection

Exposure of the photo cathode to excessive levels of irradiance causes heating, excessive dark currents, and sometimes permanent damage within the tube. To guard against accidental over exposure during

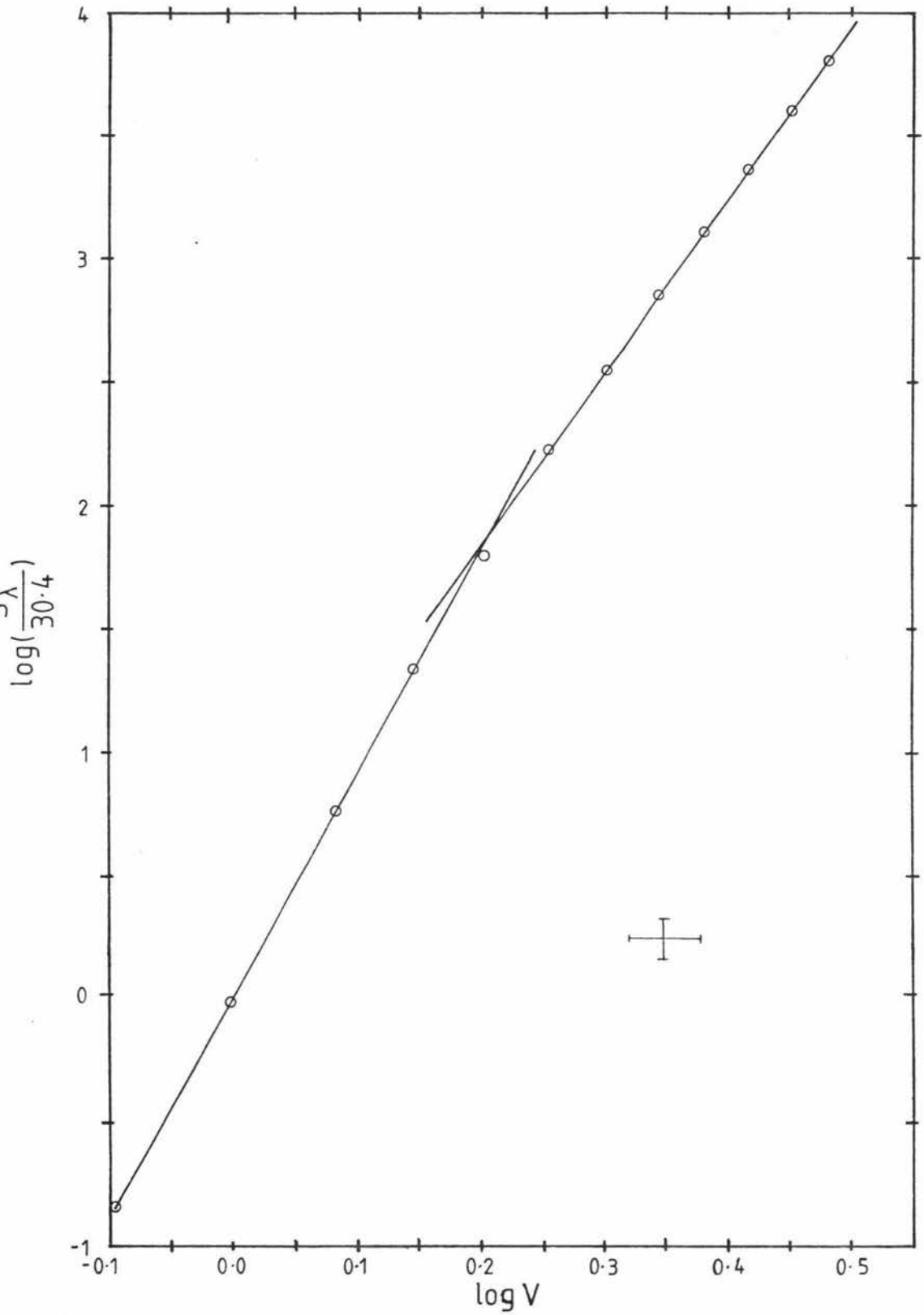

Fig :3·12 Logarithm of normalised PMT sensitivity vs logarithm of normalised output voltage.

servicing or normal operation it was considered necessary to include a high voltage shut down device which would be triggered when the high voltage applied to the PMT dropped below a certain value as a result of excessive irradiance. A maximum safe irradiance of 10^{-8} Wcm^{-2} was decided on (see Table III). Equation (3.4) indicates that this corresponds to an output voltage of 0.7 volt. To achieve a greater safety margin, and as the tube sensitivity varies by only a small proportion at low tube voltages the over exposure voltage criterion is actually set to 1.0 volt, thus explaining why $V=V_{Eht}/500$

3.4 Control electronics

A functional block diagram of the control eletronics is given in Fig: 3.13, and a semiconductor components list can be found in appendix III. An explanation of each block function follows.

High Voltage generator

The high voltage required to drive the PMT is generated by the high voltage circuitry from a Philips oscilloscope. The output of the EHT generator is 100 times the input voltage and supplies a maximum of -1500 volts at several milliamps.

Feedback circuit

IC8, IC9, Q1 and the high voltage generator comprise the feedback circuit that maintains the PMT anode current at a constant 0.2 μA. The non-inverting input of IC8 is used to sense the anode voltage. Because of its high input impedance there is no practical disturbance of this voltage. IC9 inverts the output voltage of IC8 to give the required phase of the feedback signal. Transister Q1 provides current gain to drive the high voltage generator.

Output

The PMT voltage is sensed by IC10 after being attenuated by the resistive divider of R2 and the dynode chain resistors. IC10 is an inverting buffer which provides a positive voltage output,

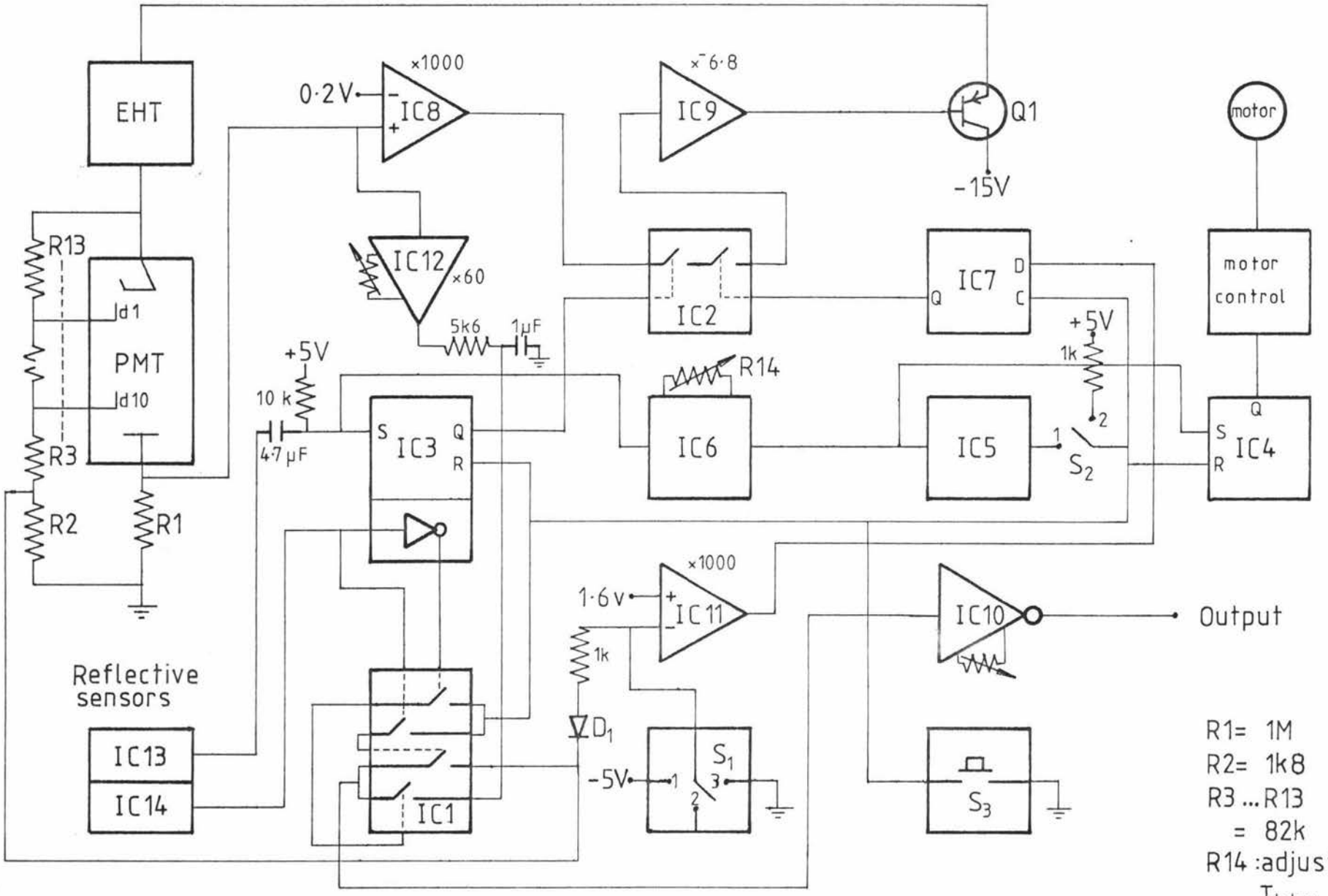

Fig:3·13 Electronics block diagram for UVB instrument.

and ensures recording devices do not affect the measured voltage. The output of IC10 can be zeroed, by use of the null offset potentiometer, when the high voltage generator is turned off.

The anode dark current is monitored as the voltage developed across R_1 when the high voltage generator applies maximum voltage to the PMT, and the photo cathode irradiance is zero.

The high impedance input of IC12 is used for the same reason as for IC8. The output voltage is filtered by the shown R C network to remove the 0.6 volt peak to peak noise signal, the source of which is the high voltage generator, the high gain feed back current and shot noise. The output voltage is then gated to IC10 when the appropriate filter wheel channel is positioned over the photo cathode. The output of IC12 is nulled manually when the high voltage generator is turned off.

Filter wheel position reflective sensor

IC13 triggers the timer (IC6), and the flip flop (IC3) which gates the analogue switch in IC2, when the reflective discs on the filter wheel are positioned above the reflective sensor. The R C trigger network of IC3 is suitably slow (time constant of approximately 50 ms) to allow for the slow fall times from the reflective sensor.

When IC14 is activated it causes the input to IC10 to be switched from the voltage across R_2 to the output of IC12, via the analogue switches in IC1. One of the NAND gates of IC3 is wired to invert the sensor voltage applied to one of the analogue switches in order to obtain the correct switching sequence.

Circuit Timing

Timer IC6 is operated in the monostable mode, with the period of the output pulse (T_{Delay}) adjusted, by R14, so that the filter wheel motor is turned off (via IC4) by the negative-going edge of the pulse when a filter is directly over the photo cathode. The negative edge of the output pulse also activates timer IC5, (wired for monostable operation) which has an output pulse, of duration T_{Sample}, which is adjustable by replacement of a capacitor-resistor timing network.

This output pulse is used to gate the control of the over-exposure latch IC7, and is also used to gate the analogue switches in IC1 that pass data to the output buffer only during sampling times. The negative edge of the pulse is applied to the reset pins of IC3 and IC4 to restart the system.

Over-exposure Protection

The comparator, IC11, senses the attenuated PMT high voltage and compares it to 1.0 volt. The output provides the data for the latch IC7 which is sampled during the time the control pin voltage is high. The latch output operates an analogue gate in IC2, so that during sampling if V<1.0 volt the analogue switch in IC2 will open, if V≥1.0 volt the analogue switch will remain closed.

Filter Wheel Motor Drive

The motor and driver electronics were purchased as a unit.

The motor drive electronics operate to stabilise the filter wheel speed by adjusting the voltage applied to the dc motor. IC4 turns the motor off during sampling by removing the voltage supply to the driving electronics.

Continuous Sampling

If continuous on-line sampling is required of any particular channel of the filter wheel, then S_2 is thrown to position 2 and the detection electronics interpret this as an indefinite extension of the sample time (Tsample). To restart cyclic operation S_2 is first thrown to position 1 and then S_3 is depressed to reset IC3 and IC4. If this sequence is not followed, the latch IC7 will see an effective over-exposure, as depressing S_3 with S_2 in position 2 will leave the control line of IC7 high. The data line andQ1 voltages will then be low, thus turning off the high voltage generator until S_1 is used to restart it and send the data line on IC7 high.

Operation of S1

During normal operation S1 is in position 2 and comparator IC11 senses the voltage developed across R_2. At switch-on the output of IC7 is low and the high voltage generator remains turned

off. To start the system in operation, S_1 is thrown to position 1 causing the output of IC7 to go high. S_1 is then returned to position 2 for normal operation. To shut down the high voltage generator, S_1 is thrown to position 3 which sends the output of IC11 low and thus opens the analogue switch in IC2. At switch-on it is also required that S3 be pressed to reset IC3 and IC4 from random power-on states.

It should be noted that operation of S_1 and S_2 should be altered only during T_{sample} after the initial switch-on sequence otherwise the switch-on sequence may need to be repeated.

Description of operation

At initial switch-on S_1 is placed in position 1, and S_2 in position 1 and S_3 depressed. Once the high voltage generator has been activated S_1 is returned to position 2 for normal operation. If over-exposure occurs the system can be restarted by working through the initial switch-on procedure. For continuous sampling it is necessary to wait until the required channel is being sampled and then place S_2 in position 2 before the sample time is complete. To restart for normal operation place S_2 in position 1 and press S_3. To shut down the instrument place S_1 in position 3 and S_2 in position 2. This will turn the high voltage generator and the filter wheel motor drive off.

Power Supplies

The electronics require four different working voltages, ±5 volts and ± 15 volts. The ± 5 volt supply operates the digital controls and some analogue electronics and the ± 15 volt supply provides the -15 volt drive to the high voltage generator. Each supply provides up to 1 amp.

To protect the PMT from being run at more than 1500 V, its maximum safe operating voltage, the -15 V power supply voltage is limited to a value that produces a PMT voltage of just below the safe value.

3.5 Electronics test results

Dark current monitor channel

The relation between the output voltage and the anode dark current was determined experimentally by setting the instrument to the dark current monitor channel, and obtaining a range of anode

currents (which were measured as the voltage developed across the anode resistor, after buffering by a high input impedance operational amplifier with an R-C smoothed output) and the respective output voltages, by allowing varying amounts of extremely low levels of irradiance to fall on the photo cathode. The results are shown in Fig: 3.14.

The circled data points are outside the linear operating range of IC12 and can be ignored because dark currents of greater than 50 nA will not be present in normal operation, and if dark currents greater than this are observed then the PMT requires cleaning, replacing, or a period of rest to remove the space charge accumulated after exposure to large irradiance levels. An interesting effect was observed during testing. The presence of small dust particles on the photocathode window caused an approximate 10-fold increase in the dark current, which decreased slowly over a period of several hours continuous running on one channel. Cleaning of the window caused the dark current to return to a normal value.

Anode current error signal

Because of the operation of a feedback circuit, and the variation of dark current with PMT gain, an error signal is always present in the monitored anode voltage. To determine the effect of this the anode current was monitored for a range of output voltages by varying the incident irradiance levels. The value of I_A found was corrected for the presence of the dark current using the expression $\frac{I_{Dark}}{Gain}$ = constant as given by the PMT manufacturer [8].

The anode dark current can be found using the experimental result that the dark current was 19 nA with a gain of 3.4×10^6 at a PMT voltage of 1450 volts.

$$\text{constant} = \frac{19 \times 10^{-9}}{3.4 \times 10^6}$$

$$= 5.6 \times 10^{-15}$$

$$I_{Dark} = 5.6 \times 10^{-6} \text{ Gain (nA)}$$

These values were then subtacted from the anode current at the corresponding output voltages and gains to give the corrected data in Fig: 3.15

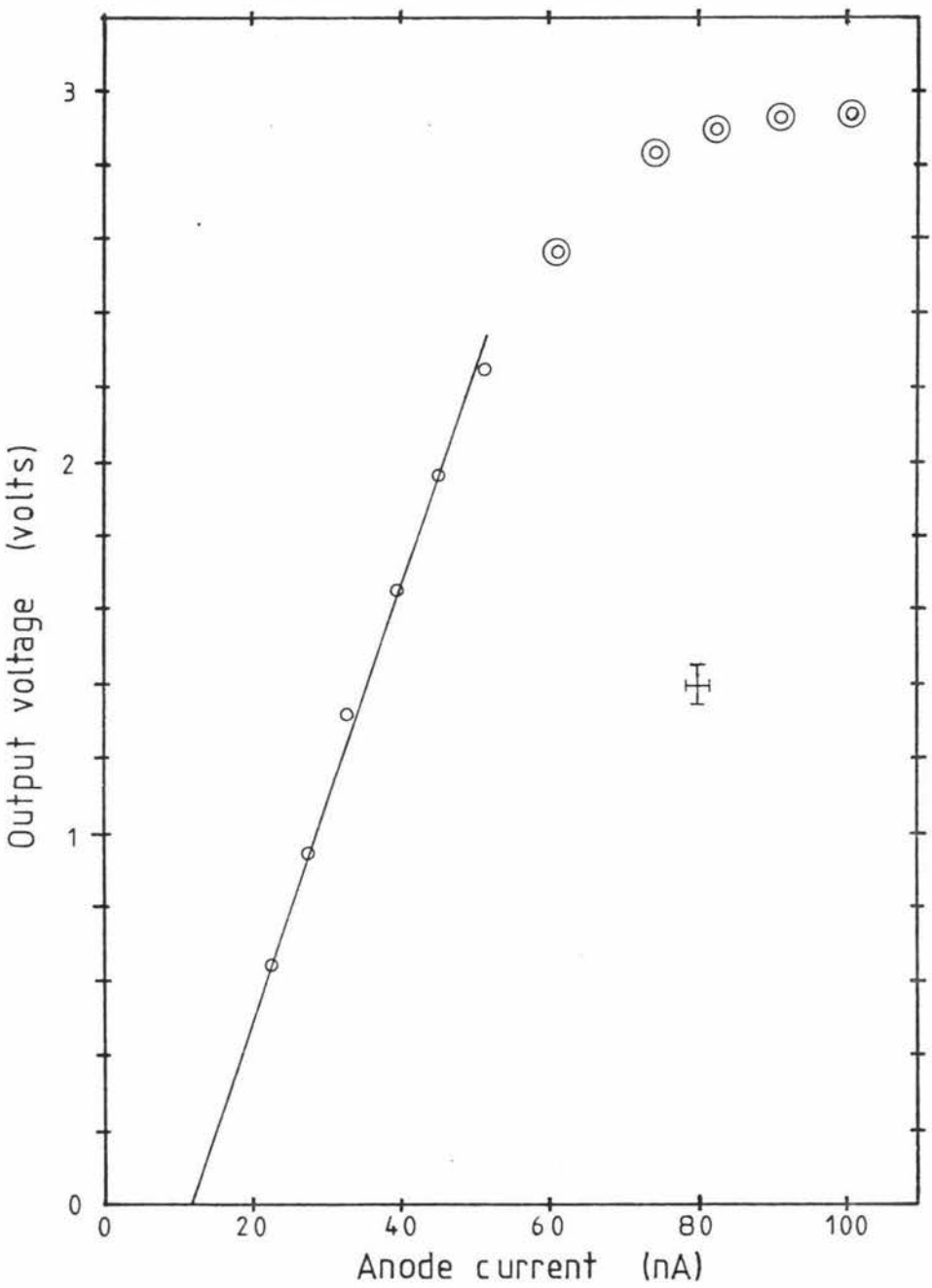

Fig:3.14 Output voltage vs anode current for the dark current monitor channel at constant EHT voltage.

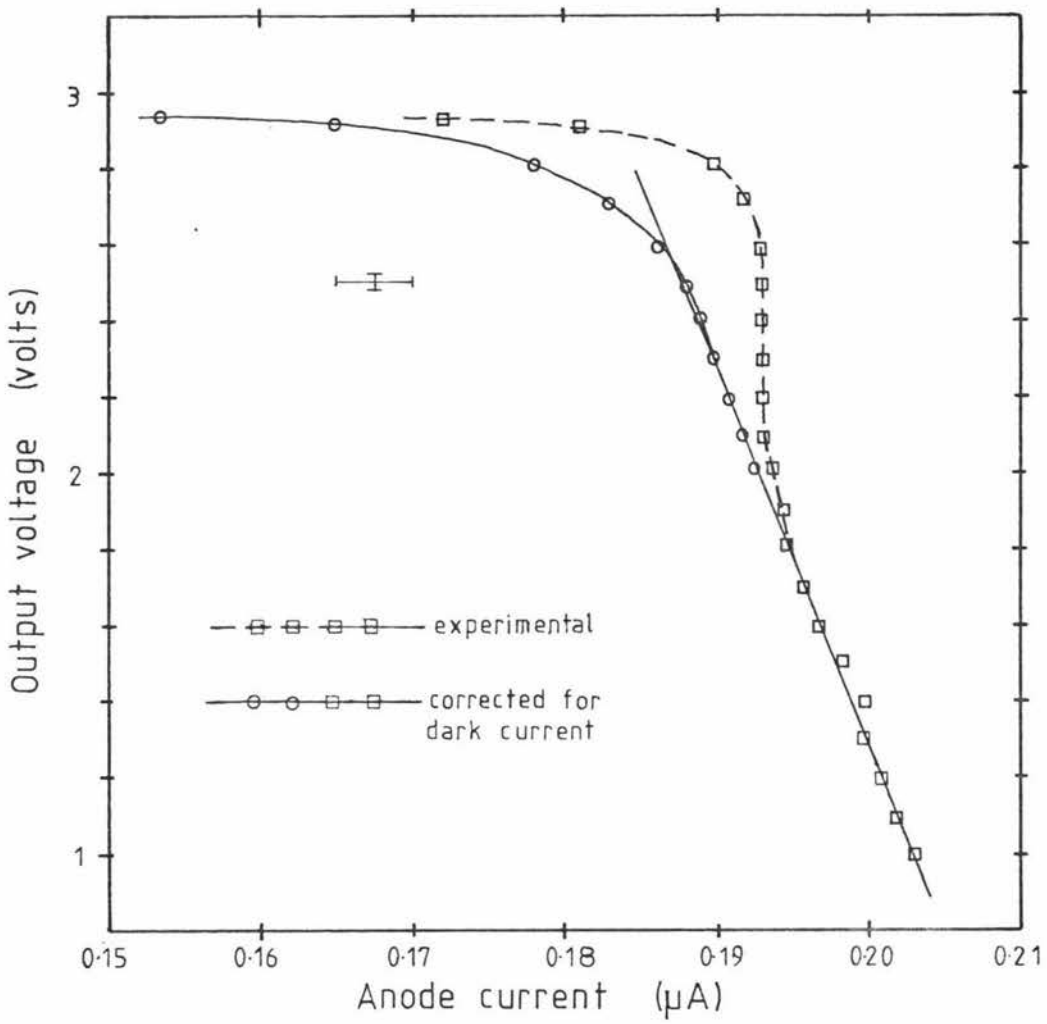

Fig:3·15 PMT transfer function in the designed mode

It should be noted that the above equation exhibits deviations from real results at high and low gain values [8]. The high gain deviations are most important because the dark current contributes some 10% to the total anode current, but for simplification of calculation the expression will be assumed valid for all gains here.

Using linear regression techniques the expression for the corrected anode current data as a function of output voltage was found to be

$$I_A = -(1.20\pm0.05)\times10^{-2}\ V + (2.17\pm0.01)\times10^{-1}\ (\mu A) \qquad (3.6)$$

For the purpose of this calculation the top three data points were omitted, and experimental data for V greater than 2.7 Volts should, therefore, be ignored. Equation (3.6) is substituted into equations (3.4) and (3.5), and substituting $A_k = 7.5\pm0.5\ cm^2$ the following are obtained,

for
$V<1.7$ volts , $E_k = \Delta F[(9.1\pm0.7)\times10^{-10} - (5.1\pm0.7)\times10^{-11}V]\ V^{-(8.8\pm0.2)}$ (3.7)

$V\geqslant1.7$ volts, $E_k = \Delta F[(4.1\pm0.9)\times10^{-10} - (1.1\pm0.3)\times10^{-11}V]\ V^{-(7.24\pm0.08)}$ (3.8)

Where E_k is the total irradiance over the band width of the filter in units of $W\ cm^{-2}$.

3.6 Calibration

From equations (3.7) and (3.8) the expression relating to the total instrument irradiance of channel n, (E_n), and the output voltage (V) can be expressed in the form

$$\log \frac{E_n}{E_{n,o}} = b \log \frac{V}{V_o} + \log a \qquad (3.11)$$

where $E_{n,o}$ and V_o are normalising values. The inverse square law for an isotropic radiator ($En \propto \frac{1}{r^2}$, where r is the source-detector distance) provides another relationship for the left hand side of equation (3.11)

$$\log \frac{E_n}{E_{n,o}} = \log \left(\frac{r_o}{r}\right)^2 \qquad (3.12)$$

Thus from equations (3.11) and (3.12), and experimentally determined values of and V, the values of b in equation (3.11) can be found by calculating the slope of a graph of $\log \left(\frac{r_o}{r}\right)^2$ vs $\log \frac{V}{V_o}$ (Fig: 3.16)
Two values of b are found which are dependant on the instrument output voltage (V). The values are:

$V<1.7$ Volts , $b = -7.60\pm0.05$

$V\geqslant1.7$ Volts , $b = -6.99\pm0.09$

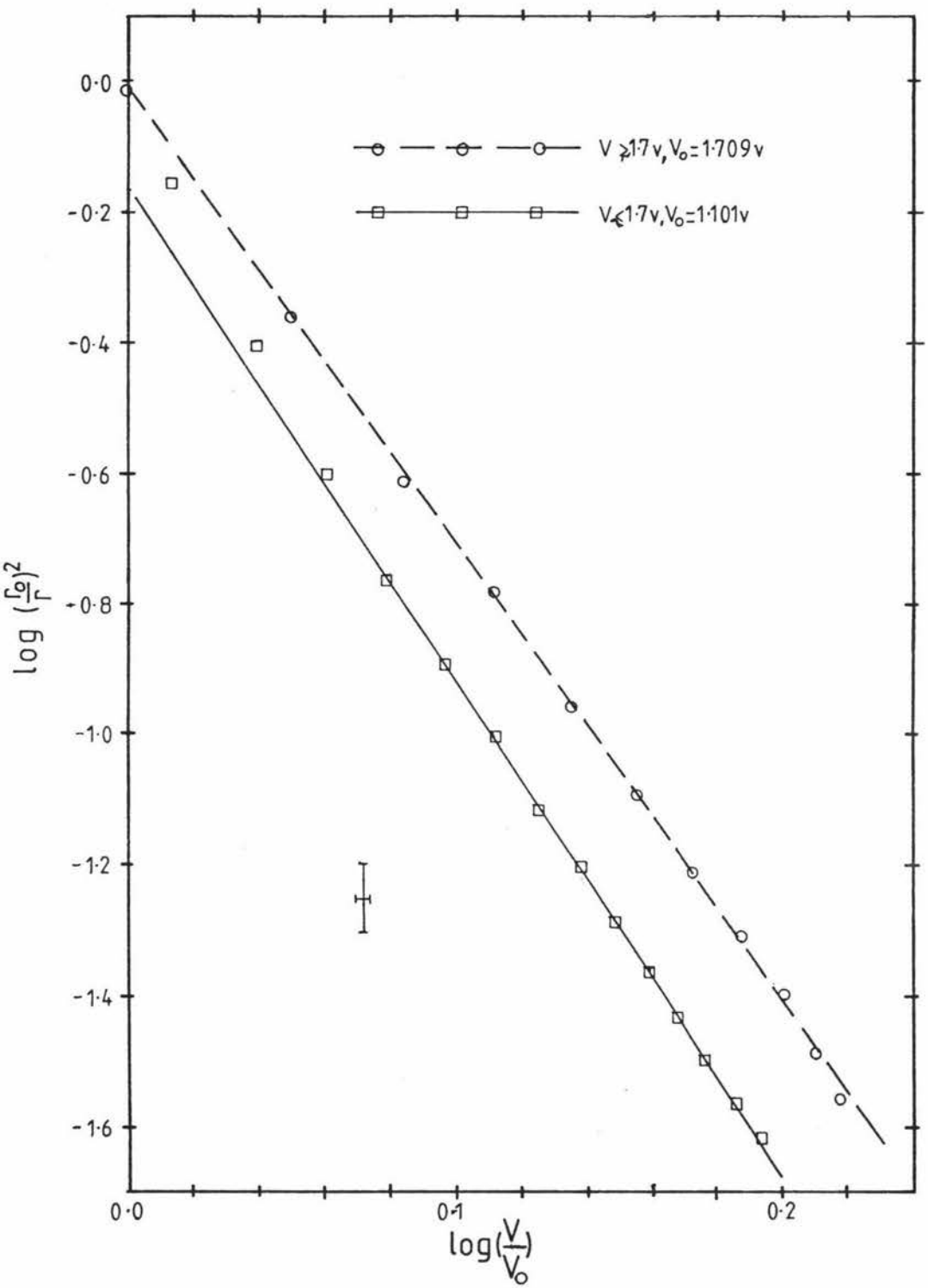

Fig:3·16 Calibration curves for the UVB instrument.

The three data points for $V < 1.7$ volts that do not lie on the line drawn are ignored in the calculation of b, as these points are at values of r which do not conform to the inverse square law for the aperture used.

The value of a in equation (3.11) was determined by calibration with a standard lamp. In order for this to be done the spectral sensitivity of the instrument was found using the experimental arrangement shown schematically in Fig: 3.17. The measurements were carried out at the Physics and Engineering Laboratories of the D.S.I.R., Gracefield.

The apparatus consisted of an Osram XBO - 450 watt Xenon lamp with a GCA/McPherson 2051, 1 meter focal length monochromator that was fitted with a pre-disperser. The exit slit was set at 1.2 mm to provide a beam with a bandwidth of 1nm.

The beam is incident directly on to the Rhodium B cell, and a remotely controlled mirror is used to reflect the beam onto the instrument for alternate readings of instrument response and relative incident irradiance. The front-surfaced mirror of aluminium vapourised on glass had an average reflectance of 0.89 ± 0.03 over the wavelength range of 280 to 400 nm. The Rhodium B fluorescing dye [13,14] was used in a photon counting arrangement and a correction factor was applied to the PMT output to convert this back to irradiance levels. As the data is for relative measurements of the spectral response the correction is made by dividing the PMT output by the wavelength of the light incident on the fluoresing dye. The Rhodium B cell was 1 cm thick and a concentration of 5 gl^{-1} in ethylene glycol was used to ensure all incident photons were collected. The PMT was an EMI 9558QA with a halon powder lined integrating sphere.

The irradiance levels of the light from the Monochromator were less than those detectable by the instrument with the diffuser and collimator fitted. Because of this, and with possible further modifications in view, the spectral response curves were measured with the collimator and diffuser removed.

Correction of the instrument output (V) was made for the non-constant incident irradiance levels and the photon counting response of the PMT by the following expression.

$$\text{Normalised relative spectral response} = \frac{V^b}{E_{pmt}} \quad \frac{E_{o,pmt}}{V_o^b \quad \lambda_o}$$

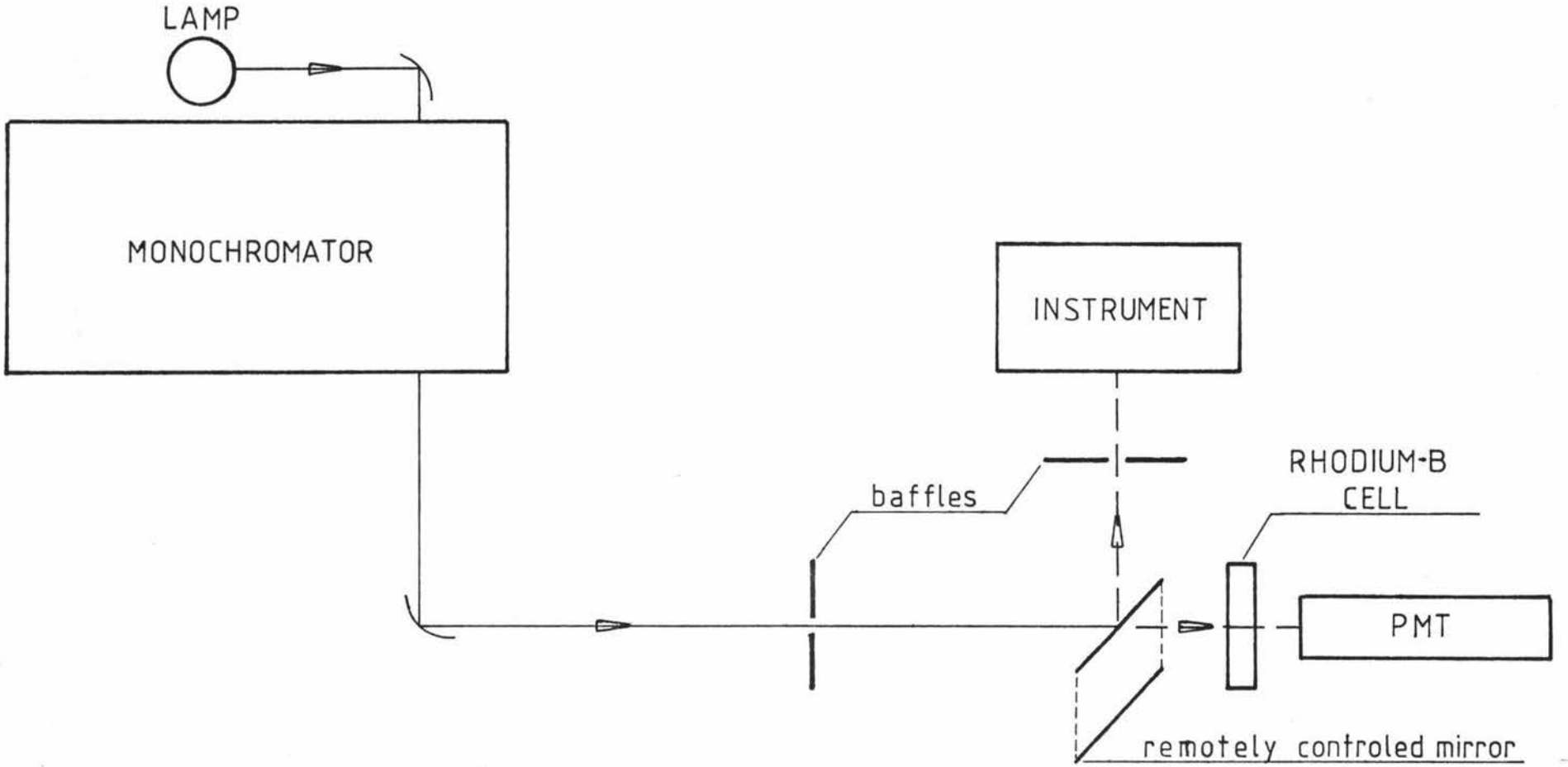

Fig:3·17 Apparatus for relative spectral sensitivity measurements.

This is derived from the relation:

$$\text{Normalised relative spectral response} = \left(\frac{E_{output}}{E_{o,output}}\right)\left(\frac{E_{instrument}}{E_{o,instrument}}\right)$$

The subscript 'O' signifies the normalising value at the wavelength of peak response of each filter channel. The results are shown in Fig: 3.18 with the upper cut-off limits shown with an expanded relative reponse scale in Fig: 3.19. The total relative spectral response of the instrument for each channel was found by multiplying the data from Figs: 3.18 and 3.19 by the combined transmittance of the protective dome, filter paper diffuser and collimator.

As the diffuser and collimator transmittance is constant, and relative measurements are sought, the normalised spectral transmittance of the dome alone was used. The resulting normalised spectral sensitivity curves are shown in Fig: 3.20. From this diagram it is apparent that data from the instrument for the 290 and 300nm channels will be meaningless because of the out-of-main-passband transmittance values near 385nm, which, when multiplied by the incident solar spectral irradiance will dominate the total irradiance measured.

The calibration constant values for each filter were found using a standard lamp with spectral irradiance values (E_λ) given in table VI. The relation between the instrument output (V) and the lamp spectral distribution is derived from

$$E_n = aV^b \qquad (3.13)$$

Where the total irradiance (E_n) of channel n is

$$E_n = \int_{\lambda_1}^{\lambda_2} S_{\lambda,n}\, E_{\lambda,n}\, d\lambda \qquad (\mu W cm^{-2})$$

$$= c \int_{\lambda_1}^{\lambda_2} S_{o,\lambda,n}\, E_{\lambda,n}\, d\lambda \qquad (3.14)$$

$$= c\ E_{o,n}$$

$S_{o,\lambda}$ is the normalised spectral sensitivity of the instrument and $E_{o,n}$ is the total irradiance of channel n after weighting by the normalised spectral sensitivity of that channel.

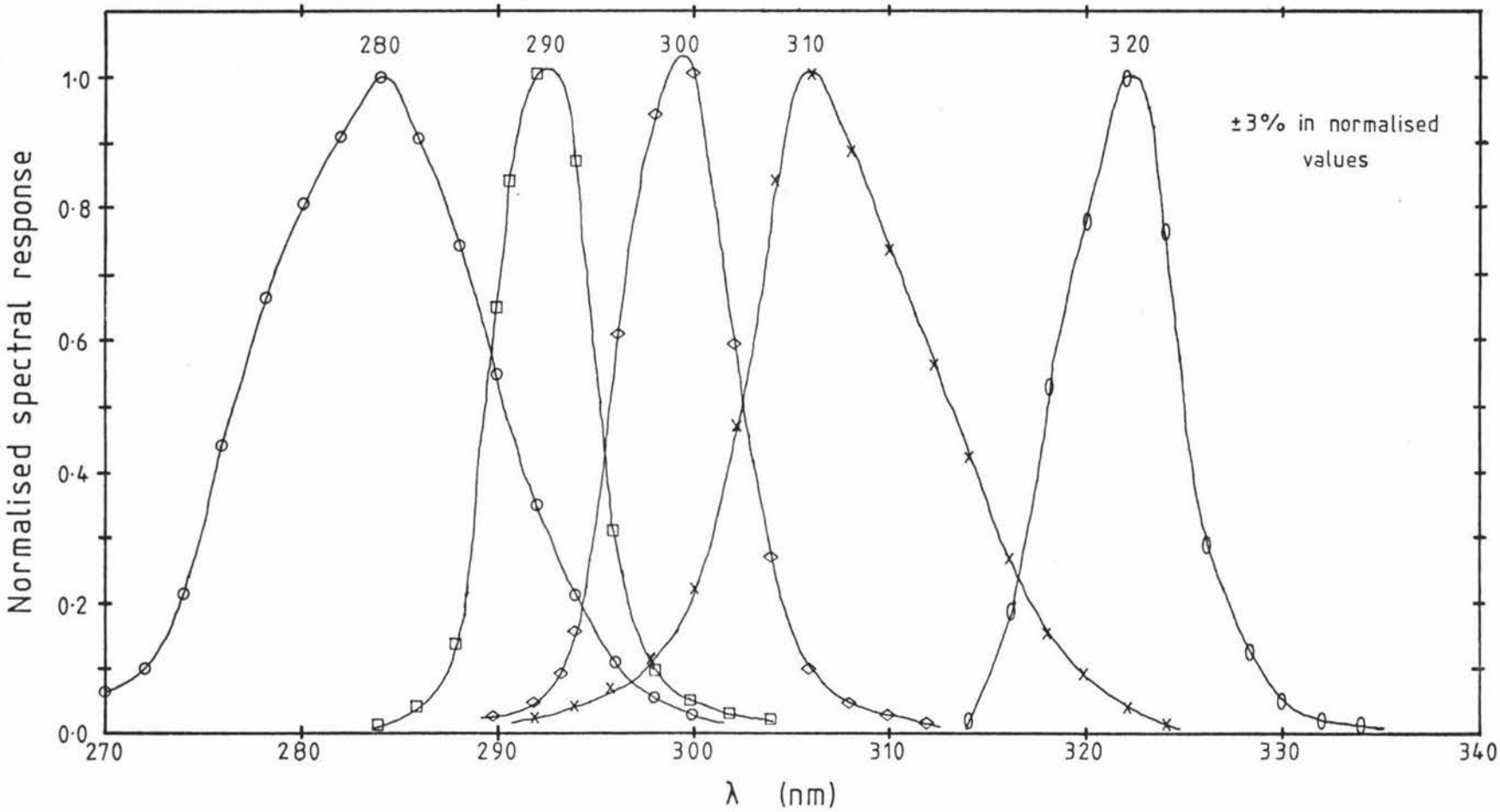

Fig:3·18 Normalised spectral response curves measured experimentally with the collimator and diffuser removed.

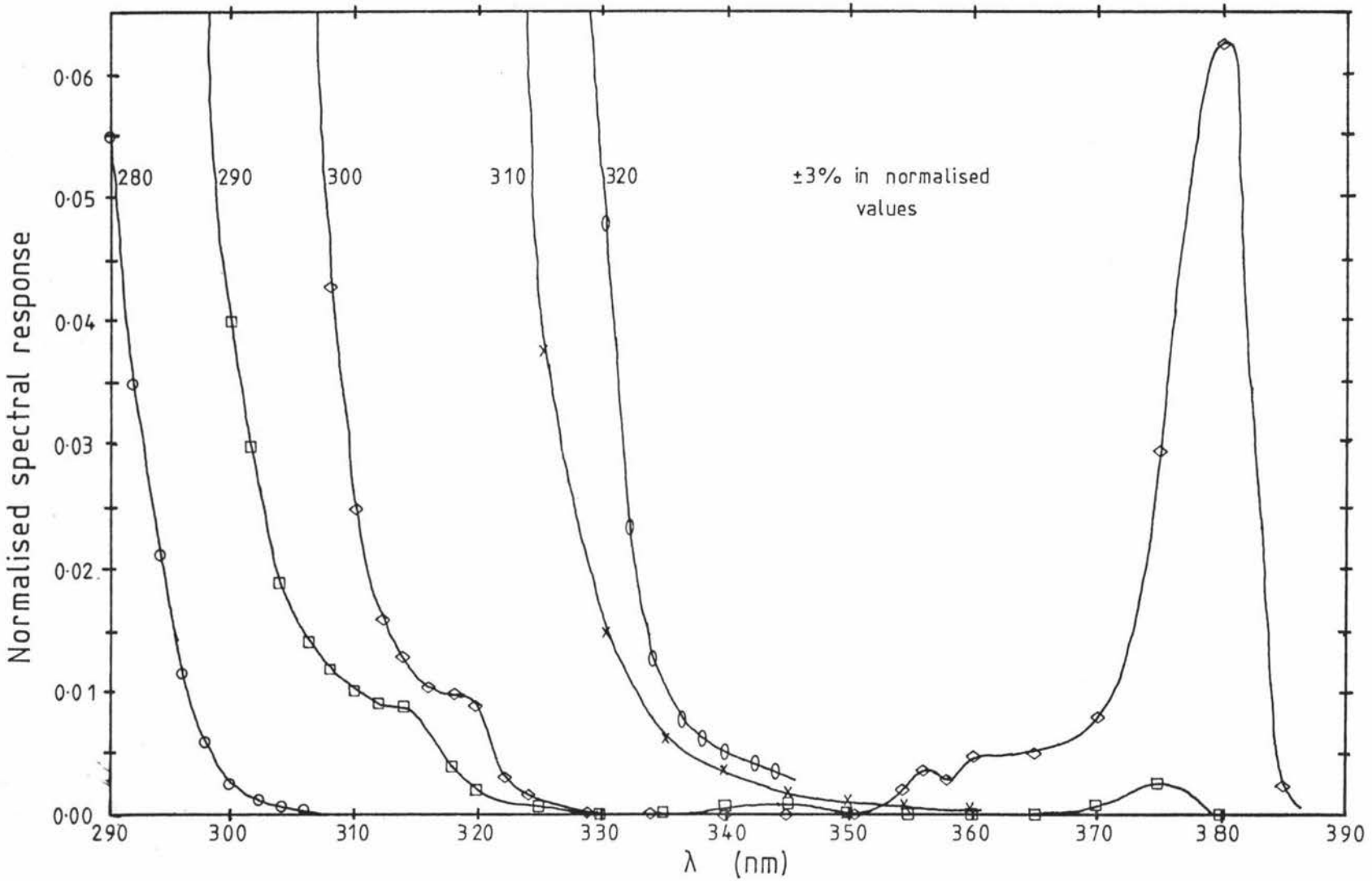

Fig :3·19 Expanded scale, upper cut-off curves from Fig :3·18.

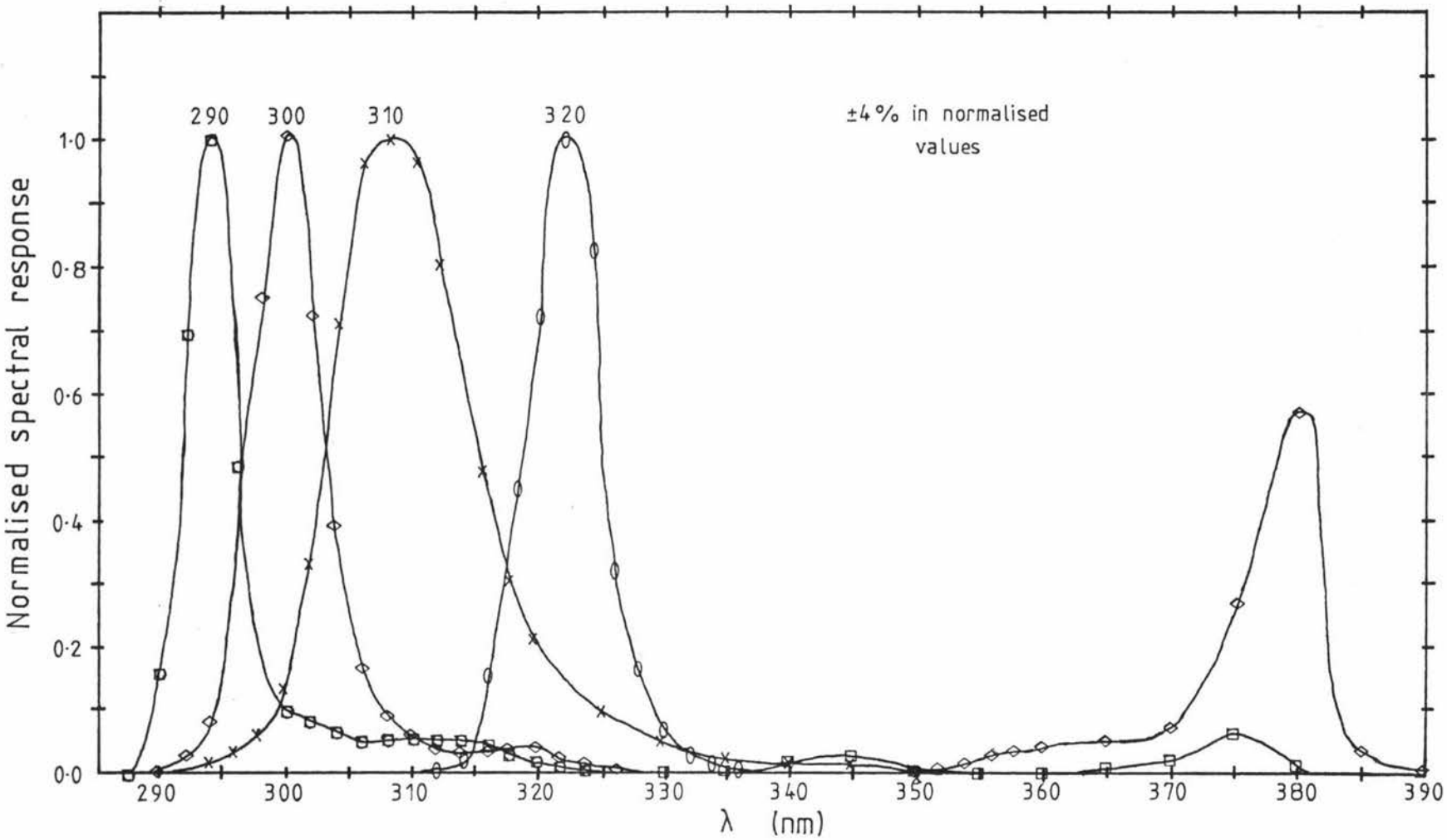

Fig:3·20 Normalised spectral response curves for the complete instrument.

The following expression for the calibration constant (K) is found from equations (3.13) and (3.14).

$$K = \frac{a}{c} = \int_{\lambda_1}^{\lambda_2} S_{o,\lambda}\ E_\lambda\ d\lambda \Big/ V^b$$

The integration value between the spectral sensitivity limits of λ_1 and λ_2 are determined from Table VI and Fig: 3.20.

Table VI

Spectral irradiance of 1000 Watt Tungsten Halogen lamp.

	Units of Wavelength (nm)									
λ(nm)	0	1	2	3	4	5	6	7	8	9
280	0.093	0.097	0.101	0.105	0.110	0.115	0.119	0.124	0.129	0.135
290	0.140	0.145	0.151	0.157	0.163	0.169	0.175	0.181	0.188	0.195
300	0.202	0.210	0.217	0.226	0.234	0.242	0.251	0.260	0.269	0.278
310	0.288	0.298	0.308	0.318	0.328	0.339	0.350	0.361	0.373	0.384
320	0.396	0.408	0.421	0.433	0.446	0.460	0.473	0.487	0.501	0.515
330	0.530	0.545	0.560	0.575	0.591	0.607	0.623	0.640	0.657	0.674
340	0.692	0.709	0.728	0.746	0.765	0.784	0.803	0.823	0.843	0.863
350	0.884	0.906	0.928	0.950	0.973	0.996	1.020	1.044	1.068	1.092
360	1.117	1.142	1.168	1.193	1.220	1.246	1.273	1.300	1.328	1.356
370	1.384	1.413	1.442	1.471	1.501	1.531	1.561	1.592	1.623	1.655
380	1.686	1.719	1.751	1.784	1.817	1.851	1.885	1.919	1.954	1.989
390	2.025	2.061	2.097	2.133	2.170	2.208	2.245	2.284	2.322	2.361
400	2.400	2.441	2.482	2.523	2.565	2.607	2.650	2.692	2.736	2.779

Spectral irradiance of 1000 Watt Tungsten Halogen lamp S-412 in $\mu W cm^{-2} nm^{-1}$ with 1% accuracy at a distance of 50 cm when operated at 8 amps.

Data is interpolated from calibration report supplied, with 10 nm intervals between data points.

The expression for calculation of the total irradiance of channel n is now

$$E_{o,n} = K\ V^b \qquad (\mu W\ cm^{-2}) \qquad (3.15)$$

The values of K determined experimentally were for V>1.7 Volts, and to determine the value of K^1 for V<1.7 Volts the following expression was used,

$$E_{o,n} = K\ V^{-6.99} = K^1 V^{-7.60} \text{ when } V = 1.7 \text{ Volts}$$

$$\therefore K^1 = 1.38\ K$$

The results for K and K^1 are given in table VII.

Table VII
Experimentally determined calibration constant values.

Filter Channel	$K \pm 3\%/10^{-3}$ ($\mu W\ cm^{-2} V^{6.99}$)	$K^1 \pm 3\%/10^{-3}$ ($\mu W\ cm^{-2} V^{7.60}$)
290nm	0.61	0.84
300nm	1.39	1.92
310nm	1.06	1.47
320nm	0.85	1.17

It should be noted, that the calibration constant values are assumed to be independent of the output voltage within the two ranges of V>1.7 Volts and V<1.7 Volts, to simplify the equations to be used in later analysis. On comparing the values in table VII with the corresponding values in equations (3.7) and (3.8), and after converting the units to $\mu W\ cm^{-2}$, it was concluded that the theoretical results are in agreement with those found experimentally. The error introduced by using the above assumption is approximately 5% as derived from equation (3.6). Thus the total error in the values of table VII when used in equation (3.15) are ± 6%.

The results for the 290 and 300 nm channels yield information of little value for solar irradiance data (as already explained) but are included for completeness. The equations for calculation of the incident irradiances are now as follows

(1) 310 nm channel

$$\begin{aligned} V \leqslant 1.7 \text{ Volts}, \quad E_{o,310} &= 1.47 \times 10^3\ V^{-7.60}\ \mu W\ cm^{-2} \\ V > 1.7 \text{ Volts}, \quad E_{o,310} &= 1.06\ 10^3\ V^{-6.99}\ \mu W\ cm^{-2} \end{aligned} \qquad (3.16)$$

(11) 320 nm channel

$$\begin{aligned} V \leqslant 1.7 \text{ Volts}, \quad E_{o,320} &= 1.17 \times 10^3\ V^{-7.60}\ \mu W\ cm^{-2} \\ V > 1.7 \text{ Volts}, \quad E_{o,320} &= 0.85 \times 10^3\ V^{-6.99}\ \mu W\ cm^{-2} \end{aligned} \qquad (3.17)$$

The accuracy in the result of $E_{o,n}$ was determined from the 6% accuracy of K, a 2% uncertainty in values of V due to drift (stable to 0.3% error over short periods of several hours), and

the error in the exponent values of V in the above equations. These yield an overall uncertainty of 15%. The main source of this error is the 2% drift in the output voltage, which is possibly due to to power supply fluctuations to the high voltage generator, caused by heating effects while in operation. Stabilisation of these effects would yield an overall accuracy in the result of 7%, a considerable improvement worth further investigation.

From equation (3.16) and (3.17) it was found that the ratio of the maximum to minimum measurable irradiance values is 1420, which is not as high as that predicted because of deviations of the actual response from those given by the manufacturer, the safety margin allowed for in the over exposure comparator, and being limited to a maximum value of the output voltage of V out=2.7 volts.

The minimum detectable irradiances for the 310 and 320 nm channels were found from equations (3.16) and (3.17) with the output voltage V = 2.7 volts, and then dividing $E_{o,n}$ by the bandwidths of the spectral response curves Fig: 3.20. The results are:

$$\frac{E_{o,310}}{\Delta F} = (8.1\pm1.2)\times10^{-2} \quad (\mu W\ cm^{-2}nm^{-1})$$

$$\frac{E_{o,320}}{\Delta F} = (16.4\pm2.4)\times10^{-2} \quad (\mu W\ cm^{-2}nm^{-1})$$

Values for the other channels are of no value as already explained.

3.7 Instrument Cosine Response

The output voltage of the instrument was recorded for a range of angles, θ, where θ is the angle from the normal at the diffuser disc of the incident irradiance (Fig: 3.21). The incident irradiance levels were calculated, and normalised at $\theta=0^{o}$ using equations (3.16) and (3.17) to obtain, for $V_o<1.7$ volts at $\theta=0^{o}$,

$$\left.\begin{aligned} V\leqslant 1.7\ \text{Volts},\ \frac{E_{o,n}}{E_{(o,n)_o}} &= \left(\frac{V}{V_o}\right)^{(-7.60\pm0.05)} \\ V>1.7\ \text{Volts},\ \frac{E_{o,n}}{E_{(o,n)_o}} &= \frac{K\,V^{(-6.99\pm0.09)}}{K^{1}V_o^{(-7.60\pm0.05)}} \end{aligned}\right\} \quad (3.18)$$

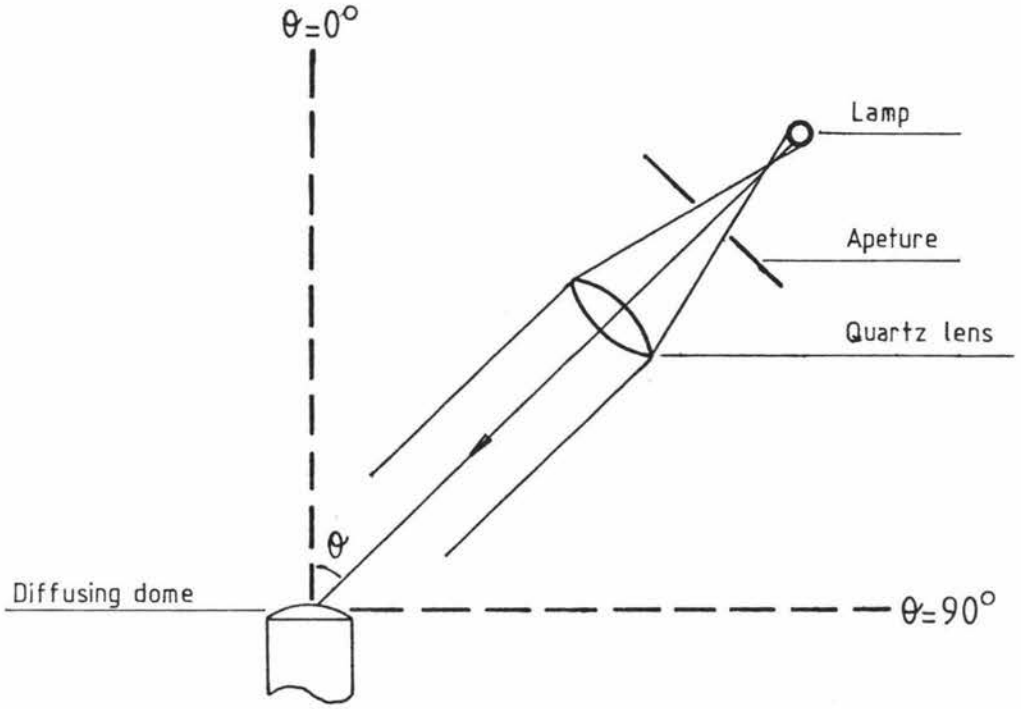

Fig :3·21 Apparatus for cosine response evaluation.

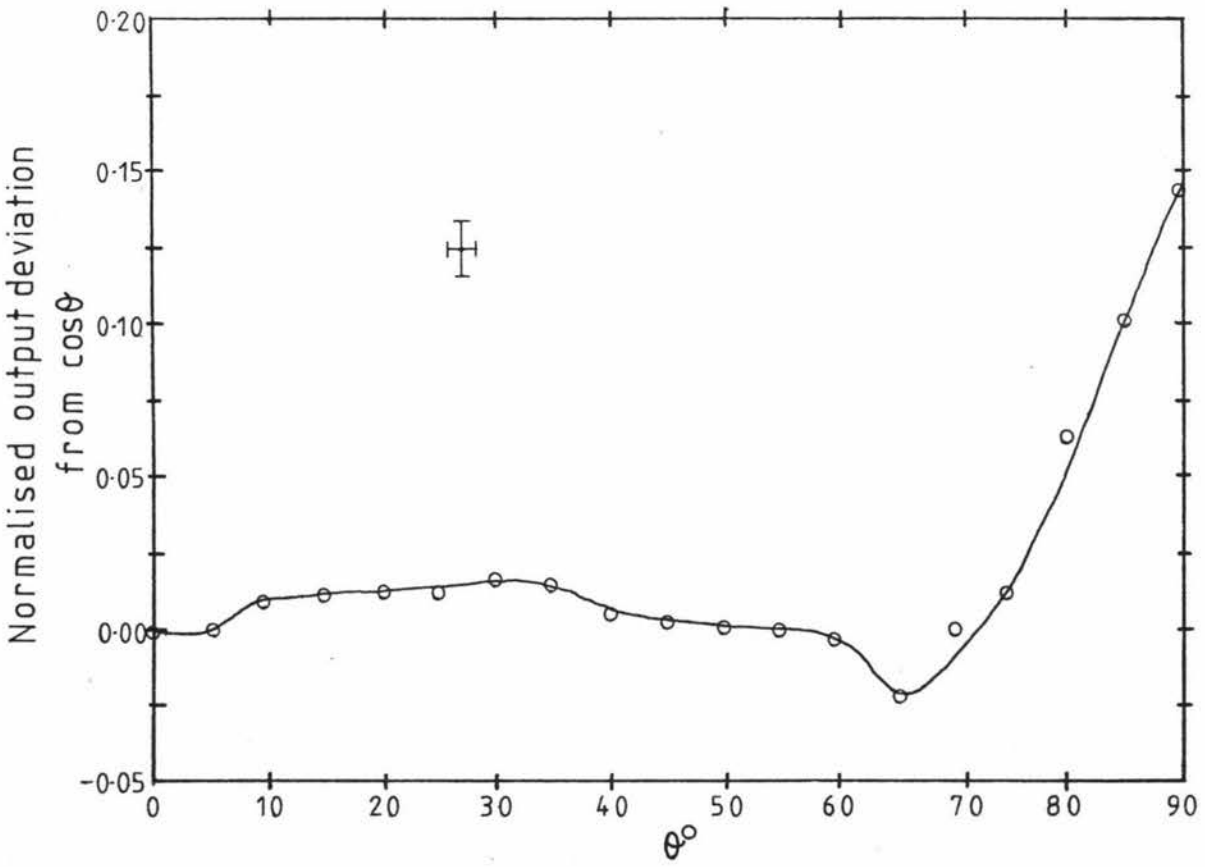

Fig :3·22 Cosine response of UVB instrument.

Cosθ was then subtracted from this normalised value to provide the difference of the collector response from the ideal and is shown in Fig: 3.22. The results show good agreement and the assumption that the diffuser acts as a flat plate collector is valid.

3.8 Data analysis procedure

The spectral solar irradiance at the instrument can be calculated from the following equation.

$$E_{s,n} = \frac{FF_n}{\Delta F_n} E_{o,n} \qquad (3.19)$$

Here ΔF_n is the bandwidth of channel n. $E_{s,n}$ is the average spectral solar irradiance received for channel n, and $E_{o,n}$ is the total irradiance of the instrument after weighting by the normalised spectral sensitivity curves. FF_n is the Filter factor [9] for the normalised spectral response curves of Fig: 3.20, and is calculated from the following expression

$$FF_n = \int_{\lambda_1}^{\lambda_2} E_\lambda \, d\lambda \quad \left[\int_{\lambda_1}^{\lambda_2} E_\lambda \, F_\lambda \, d\lambda\right]^{-1} \qquad (3.20)$$

F_λ is the spectral response at wavelength λ and E_λ is the spectral irradiance at the filter. λ_1 and λ_2 are the limits of the spectral response curves and are usually defined as being the wavelength at which $F_\lambda = 0.01$. However, because of the nature of the solar irradiance spectral the values of λ_1 and λ_2 should be found by considering the spectral response curves multiplied by the incident spectral irradiance (Figs: 3.4 and 3.5). FF_n can be calculated numerically from equation (3.20). Tables of λ, F_λ, E_λ and $F_\lambda E_\lambda$ would be used in the procedure.

Procedure for calculating E

As the function E_λ is not known "a priori" an approximation must be used in calculating FF_n. It is usually assumed that the spectral sensitivity curves are quasi-rectangular i.e. F_λ is constant over the bandwidth of the function. Thus $FF_n = \frac{1}{F_\lambda}$ and the approximated points for the function E_λ can be graphed. Alternatively values of E_λ already obtained from previous data can be used as the first approximation, for example data from Fig: 3.6 can be used.

The process now involves finding new values of $E_{s,n}$ using equation (3.19) and plotting a new approximation of E_λ, and using this new approximation again in equation (3.19) to find a better approximation to E_λ. This iterative process is continued until the new approximation of E_λ is, within a defined error difference, the same as the function used to find the new approximation. To plot the graph of E_λ, the calculated values of $E_{s,n}$ are plotted at the wavelength of the peak valve obtained from $S_{o,\lambda}\ E_\lambda$ for each channel (Fig: 3.10).
Because of the complexity of these calculations it is desirable that a computer programme be used for data analysis, the development of which is beyond the scope of this thesis.

3.9 Experimental Data

Data shown in Figs: 3.23, 3.24 and 3.25 were calculated using equations (3.18) derived in section 3.7 and represent the total irradiance received for each channel as a function of time. The data were normalised for ease of comparison between channels. The approximate spectral irradiance $E_{\lambda,o,n}$ is found from the normalised data from the expression $E_{\lambda,o,n}$ = p x normalised data,
where p is found in table VIII and has units $\mu W\ cm^{-2}\ nm^{-1}$

Table VIII
Denormalisation factors for UVB experimental data

	Figure		
Filter Channel	3.23	3.24	3.25
310nm	15	22	1.3
320nm	49	64	5.2

Values of p were found from the expression

$$\text{for } V_o \leq 1.7 \text{ Volts}, \quad p = \frac{K^1 V_o - 7.6}{\Delta F}$$

$$\text{for } V_o > 1.7 \text{ Volts}, \quad p = \frac{K\ V_o - 6.99}{\Delta F}$$

using the quasi-rectangular approximation for FF_n.

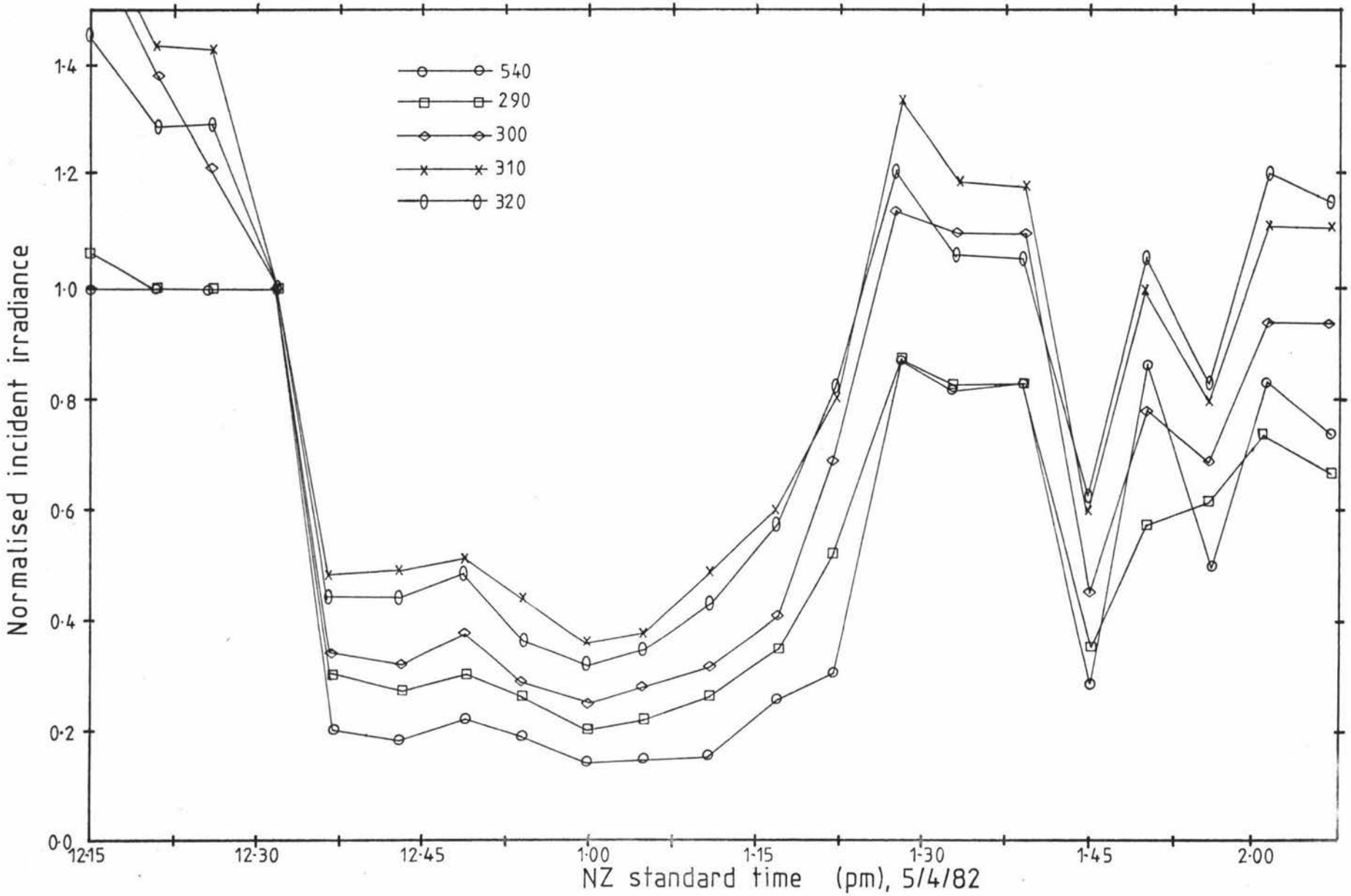

Fig:3·23 Experimental data normalised at the zenith.

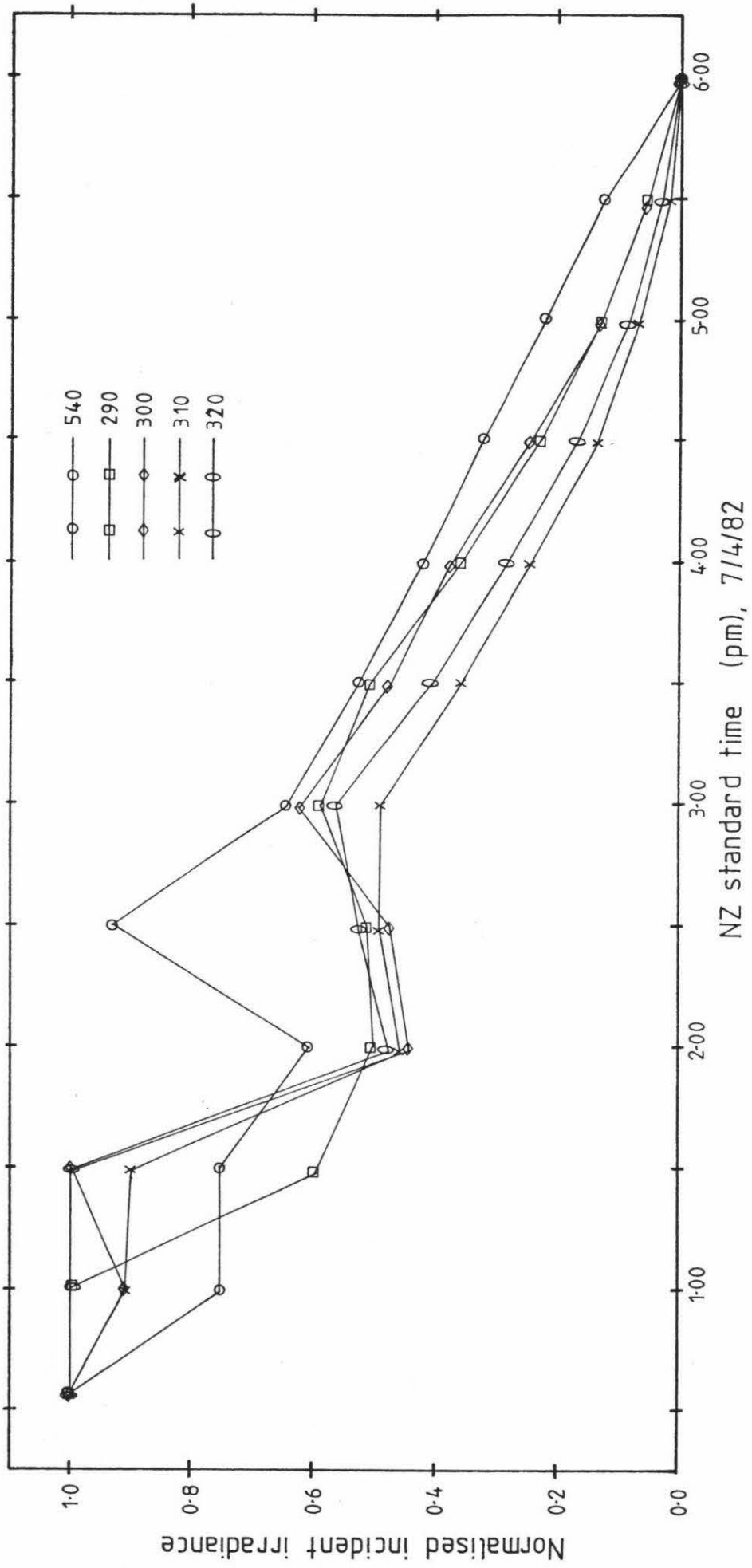

Fig:3·24 Experimental data normalised at the zenith.

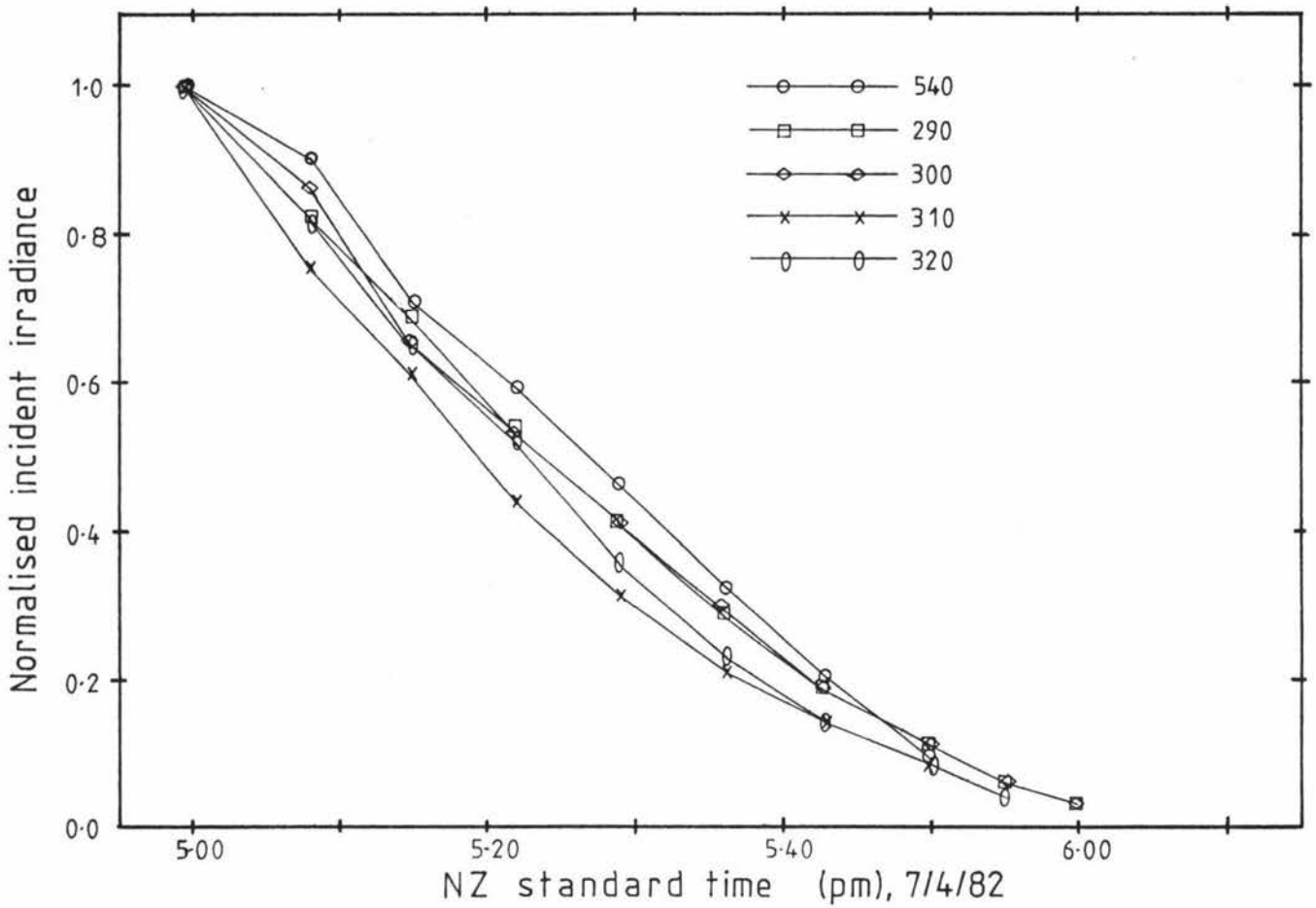

Fig :3·25 Experimental data normalised at 5pm

(sunset was at 6·01pm with clear sky conditions).

It was found that data from Fig: 3.23 gave values of approximately

$E_{\lambda,310} = 22\mu Wcm^{-2}\ nm^{-1}$ (Robinson:$10\mu Wcm^{-2}\ nm^{-1}$)

$E_{\lambda,320} = 64\mu Wcm^{-2}\ nm^{-1}$ (Robinson:$40\mu Wcm^{-2}\ nm^{-1}$)

which compare well with data by Robinson Fig: 3.6 considering the cloud present for Fig: 3.23 data, the difference in altitudes of the two observing stations, and that the instrument values were calculated using a quasi-rectangular approximation. It should be noted that the time for one filter wheel revolution is 1.4 minutes (8.5 seconds between channels with a 2 second sampling time) and the presence of small broken cloud moving at high speed will produce readings from each channel which are not directly comparable with those obtained from clear sky or reasonably static cloud cover. For ease of plotting data in Figs: 3.23, 3.24 and 3.25 all channels have been plotted at the same time scale, which is valid for long time scale data. Data from the 290 and 300 nm channels shown should really be considered as 380 nm (UVA) data for reasons already explained. It was also predicted that data from these channels would be the same after considering the pass-band of the 380 nm lobes in Fig: 3.20. This is confirmed by data presented in Figs: 3.24 and 3.25.

From the graphs it is observed that all channels indicate similar changes in irradiances for the same conditions. Discrepancies can be attributed to differing cloud transmittances and focussing effects at different wavelengths as illustrated in Fig: 3.23. Different scattering coefficients and intensity distributions in the scattered radiation (with wavelength) will also affect cloudy sky readings, as will varying irradiance values for different solar angles. This is apparent in Figs: 3.24 and 3.25. Evidence of Rayleigh scattering is clearly seen in Fig: 3.24 as a difference in the rate of change of irradiance levels for different channels. Remembering that the passband of the 280 and 290 nm filters is near 380 nm, it is observed that the nomralised incident irradiance as a function of decreasing solar angle becomes more curved as the wavelength sampled is decreased. This curving is explained as an increase in the ration of diffuse to direct irradiance received as the solar angle decreases. The effect becomes more pronounced as wavelength decreases indicating greater scattering at shorter wavelengths. Due to the presence of early afternoon cloud in Fig: 3.24, there is some uncertainty in the validity of the

normalising value being the actual maximum for all the channels and, therefore, a direct comparison between the curves is not possible. It is hoped that more data will be collected to further investigate all of the above effects.

CHAPTER 4

Conclusions

This thesis has provided a basis of design for an instrument to monitor the UVB in discrete bands. Modifications are needed to improve the quality of data recorded, but are beyond the scope of this thesis.

Such modifications should include the use of a diffusing dome with a near constant transmittance across the UVB wavelenghts. The diffusing material should also be stable over long periods of time, unlike filter paper which discolours after prolonged exposures. The use of a quartz diffuser as described in chapter 2 will meet these requirements as well as providing a good cosine response as is also outlined in chapter 2. The interference filters require a much higher out-of-main-passband rejection, which can be improved by the use of blocking filters, the use of a detector with a suitable long wave length cut-off response, and the use of high quality interference filters with no out-of-main-passband transmittance lobes on long wavelength side of the passband. Also the stacking of identical interference filters, as outlined by Goldberg and Klein [15] , increases the main passband to out-of-main-passband ration by approximately 3 order of magnitude, at the expense of lower overall spectral transmittance of the main passband, thus requiring a more sensitive PMT to provide the same amounts of irradiance resolution.

The range of the instrument response for any one channel in the constant current mode operation of the PMT gave a value of 1420 for the ration of the maximum to minimum measurable irradiances, whereas the constant voltage mode would give a ratio of approximately 500, allowing for a maximum of 10% dark current in the anode current. The constant voltage mode offers more accurate results at the expense of range of measurable incident irradiances, therefore the choice is made depending on the designer's requirements. The use of a more sensitive PMT such as a 9634QB [8] would provide 10 times the above measurement range for the constant current mode, but no greater range for the constant voltage modes.

The instrument does meet the requirements of being portable as is not the case for the much heavier monochromator based instruments, which, although providing far superior results, are more complicated

and require specialised technicians in their operation. A good example of such a monochromator based instrument is the ultravoilet submersible spectroradiometer of Smith et. al. [15]

It is not considered that the designed instrument output should be linearly related to the irradiance levels because of the data loggers and computers available which are capable of performing this function during data analysis.

It was also considered, on reflection, that an extra channel to monitor the UVA should be incorporated in the instrument, as this would be easily accomplished mechanically, and would provide UVA data without the need of another instrument.

The UVA pyranometer that has been constructed is a valuable piece of equipment in that it provides valid data at a low cost in comparison to other currently available units. The pyranometer is easily maintained and operated, and as accurate as its counterparts. It is hoped that more research will take place in this field to increase our understanding, and provide long term data as a basis on which predictions on fluctuations in UV irradiances can be made.

APPENDIX I

Vacuum Photoemissive Tube 92AV Specifications [7]

Anode supply Voltage (Max)	100 V
Luminous sensitivity	45 μA/lm
Spectral response curve	type A (S 11)
PHOTOCATHODE	
Surface	Caesium antimony
Projected sensitive area	2.1 cm^2
CHARACTERISTICS	
Anode supply Voltage	85 V
Anode series resistor	1.0 MΩ
Dark current	$\leqslant$0.05 μA
CAPACITANCE	
C_{a-k}	0.9 pF
RATINGS (absolute maximum system)	
$V_{a(b)}$ max	100 V
I_k max	25 nA/mm^2
T_{amb} max	70 ^oC

APPENDIX II

Photomultiplier Tube 9656 QB Specifications [8]

Nominal cathode diameter			44 mm
Cathode type			S-13
Window material			Spectrosil (fused silica)
Dynodes		10 stage; Venetian blind with CsSb Secondary emitting surface	
Cathode to D_1 maximum rating			300 V
Cathode to D_1 recommended rating			150 V
Cathode to Anode maximum rating (subject to not exceeding 500 A/lm)			2000V
Overall sensitivity	Rated		50 A/lm
	Max		500 A/lm
Maximum anode current			1 mA
Maximum anode dissipation			1 W
Maximum tolerable Cathode current			0.3 μA
Maximum tolerable Cathode current density			0.02 $\mu A/cm^2$
Maximum operating temperature			60°C
Minimum operating temperature			-80°C
Anode pulse rise time			6 ns
Anode pulse f.w.h.m.			18 ns
Transit time			48 ns
Capacitance, anode to all dynodes			8 pF
Dark current shot noise typical (λpeak)			$5x10^{-16}$ W
Cathode sensitivity	Minimum		50 μA/lm
	Typically		70 μA/lm
Overall sensitivity - 50 A/lm - Overall Voltage		max.	1650 V
		typical	1200 V
- Dark Current		typical	2 nA
		max.	15 nA
- 500 A/lm - Overall Voltage		max.	-
		typical	1700 V
- Dark Current		typical	20 nA
		max.	-

Pin connections. (viewed from below starting left (clockwise) of short pin/key)

1	2	3	4	5	6	7	8	9	10	11	12	13	14	15	16	17	18	19
IC	D1	D2	D3	D4	D5	D6	D7	D8	D9	D10	A	IC	IC	IC	IC	IC	IC	K

Key: IC = internally connected
Dn = Dynode n
A = Anode
K = Cathode

Socket type	B19A
μ-metal shield type	PS6B

APPENDIX III

UVB instrument semiconductor components list.

Q_1	TIP125	Darlington PNP transistor
D_1	IN914	Signal diode
IC1-2	4066	Quad analogue switch
IC3-4	4011	Quad NAND gate
IC5-6	555	Timer
IC7	4042	Quad Latch
IC8-12	3140	CMOS operational amplifier
IC13-14	OPB706c	LED - Phototransistor reflective sensor

BIBLIOGRAPHY

1 SOLAR Radiation
Edited by N. Robinson. Amsterdam, Elsevier, 1966. 347 P.

2 THE Middle Ultraviolet: Its Science and Technology
Edited by A.E.S. Green. New York, J. Wiley and Sons Inc, 1966. 390 P.

3 COULSON, Kinsel L.
Solar and Terrestrial Radiation New York, Academic Press 1975. 322 P.

4 BARTON, I.J.
The Physics and Measurement of Solar Ultraviolet Radiation.
Australasian Physical Sciences in Medicine. 199-204
Vol. 2-4, May, 1979. No. 81

5 KLEIN, W.H. and Goldberg, B.
Monitoring UVB Spectral Irradiances at Three Latitudes.
International Solar Energy Congress, New Delhi. 400-414
Vol. 1, 1978

6 DRUMMOND, A.J. and Herbert, A.W.
Instrumentation for the Measurement of Solar Ultraviolet Radiation. Reprint Series No. 38 from, The Biological Effects of Ultraviolet Radiation, Oxford and New York, Pergamon Press, 1969. 391-407

7 CATHODE Ray Tubes and Photoemissive Devices.
Mullard, Vol. 3, Part I, November 1968.

8 PHOTOMULTIPLIER Tubes
EMI Electronics Ltd., 1979. 64 P.

9 HARRIS, L.
Filters for the Isolation of Radiant Energy
The Epply foundation for research, Monograph series, No.2 June 1970. 186 P.

10 OPTICAL Filters, Interference Filters
Schott product information No. 3711e, 4 P.

11 BASHER, R.E.
Stratospheric Circulation: A Narrowband Filter Spectrphotometer for Total Ozone Determination.
Thesis, PhD., Canterbury University, 1975. 201 P.

12 KEENE, J.P.
Fatigue and Saturation in Photomultipliers.
The Review of Scientific Instruments. Vol.34, No.11,1220-1222, November 1963.

13 MELHUISH, W.H.
Calibration of Spectrofluorimeters for Measuring Corrected-Emission Spectra. Journal of the Optical Society of America. Vol.52,No.11, 1256-1258, November 1962.

14 MELHUISH, W.H.
Modified Technique for Determining the Wavelength - Sensitivity Curve of a Spectrofluorimiter.
Journal of Applied Optics. Vol.14, No.1, 26-27, January 1975.

15 GOLDBERG, B. and Klein, W.H.
Radiometer to Monitor Low Levels of Ultraviolet Irradiance
Journal of Applied Optics. Vol.13, No.3, 493-496 March 1974.

16 SMITH, R.D. et. al.
Ultraviolet Submersible Spectroradiometer.
SPIE Vol.208, Ocean Optics VI,127-140, 1979.